

1.3 Aims

To synthesize and study antimicrobial properties of ruthenium (II) complexes of Isoniazid Schiff base ligands and the free ligands.

1.4 Objectives

The objectives are;

1. The synthesis and characterization isoniazid Schiff-base ligands.
2. The synthesis and characterization of ruthenium (II) complexes of isoniazid Schiff base ligand
3. To test the compounds against *Staphylococcus aureus*, *Methicillin resistant Staphylococcus aureus* and *Pseudomonas aeruginosa*

Chapter 2: Experimental section

2.1 General remarks

All reactions were carried out under inert or nitrogen atmosphere using a dual vacuum/nitrogen line and standard Schlenk techniques unless stated otherwise. The solvents used were purified by heating at reflux under nitrogen in the presence of a suitable drying agent and stored with activated molecular sieves in tightly sealed solvent bottles. Diethyl ether was dried over sodium wire and benzophenone under nitrogen. Methanol and ethanol were dried from magnesium. Anhydrous magnesium sulphate (MgSO_4) was the drying agent. All reagents were purchased from Sigma Aldrich (South Africa) and were analytical grade. They were used as purchased without further purification. These reagents were; 2-hydroxy-5-methylbenzaldehyde (98%), 2-hydroxy-5-nitrobenzaldehyde (98%), 2-hydroxy-5-methoxybenzaldehyde (98%), 5-bromo-2-hydroxybenzaldehyde (98%), 5-chloro-2-hydroxybenzaldehyde (98%), ruthenium (III) chloride hydrate (99.9 %), dimethyl sulfoxide (98%).

2.2 Instrumentation

The ^1H NMR and ^{13}C NMR experiments were conducted on the Bruker Avance IIIHD Nanobay 400 MHz spectrometer at room temperature (298K) equipped with a 5 mm BBO probe (400

MHz for ^1H and 100 MHz for ^{13}C). Standard 1D and 2D pulse programs were used to acquire the NMR spectrum. The ^1H NMR spectra were referenced internally using the residual CD_3OD and $\text{DMSO } d_6$, and reported relative to the internal standard tetramethylsilane (TMS). Chemical shift values are given in ppm.

The FTIR spectra in solution were recorded with Perkin-Elmer Spectrum 100 Series FTIR spectrometer using KBr pellets for solids. Ultraviolet visible (UV-Vis) studies were carried out using a Nicolet100 spectrophotometer. Melting point of synthesized compounds was determined using open capillaries using SMP10 melting point apparatus. Server 1112 Series Elemental Analyzer at the University of Stellenbosch central analytical facility was utilized to perform the carbon, hydrogen and nitrogen analysis. The thermogravimetric analysis (TGA) was performed using Perkin Elmer Pyris thermal analyzer at the University of the Western Cape.



2.3 Characterization techniques

2.3.1 Fourier transform infrared spectroscopy (FTIR)

Fourier transfer infrared spectroscopy is a method used to ascertain quantitatively and qualitatively the characteristics of infrared-active molecules in organic or inorganic solids, liquids and gas samples. It is a quick and low cost technique used to analyze solid samples that are amorphous, films, crystalline or microcrystalline [59]. The scale of samples analyzed ranges from microns to kilometers and sample preparation are relatively easy.

Best IR spectra are achieved when appropriate choices are made regarding the IR source, the detection method and accessories. Moreover the analyst has to be aware of the infrared spectrum region in which the sample has its characteristic functional groups [59, 60]. The functional groups of interest in this study are the imine functional group (C=N) and the amide carbonyl functional group (C=O).

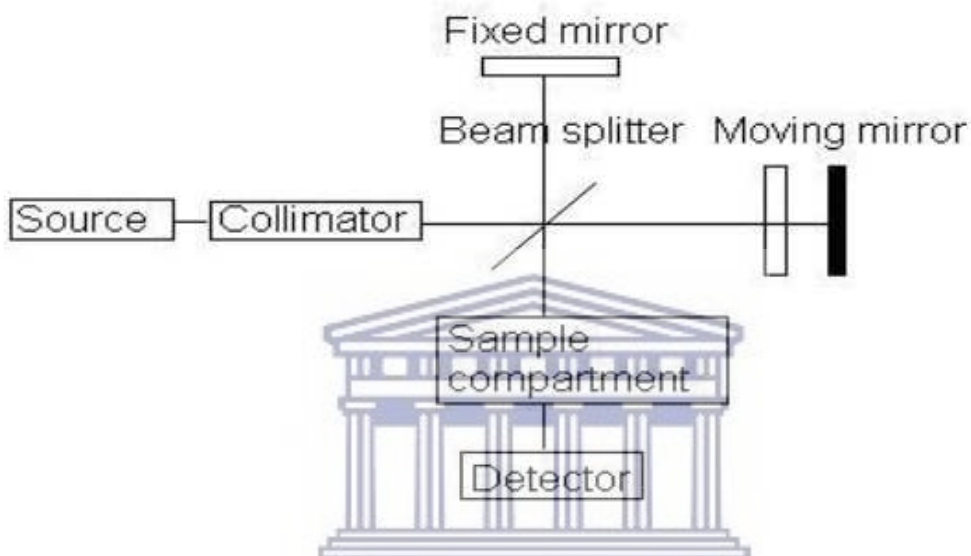


Figure 2-1: Diagram of a FTIR spectrometer [60].

UNIVERSITY of the
WESTERN CAPE

2.3.2 Ultra violet – Visible spectroscopy

Ultra violet – visible spectroscopy is a technique that investigates the variation in the electronic energy levels in a compound caused by the transfer of electrons from π or non bonding orbitals. It normally gives information about π electron systems, aromatic compounds, conjugated unsaturations and conjugated non – bonding electron systems [61]. The ultraviolet region

covers the range of 190 nm to 380 nm and the visible region ranges from 380 nm to 750 nm.

The energy diagram below (figure 8) highlights the possible transitions.

The cuvette containing the sample as well as the reference cuvette is subjected to a series of light wavelengths deriving from the spectrometer emitting an energy that matches the probable electronic transition within the molecule. Some of the light energy is absorbed as an electron moves to a higher energy level or orbital in the ultraviolet and visible regions of the electromagnetic spectrum [62]. The UV – Vis instrument analysis results in a spectrum or a graph of absorbance versus wavelength. The UV – VIS spectrum data or observed bands are not specific enough for sample identification or isolation, but can be used as mean of comparison against known compounds in a database [62].

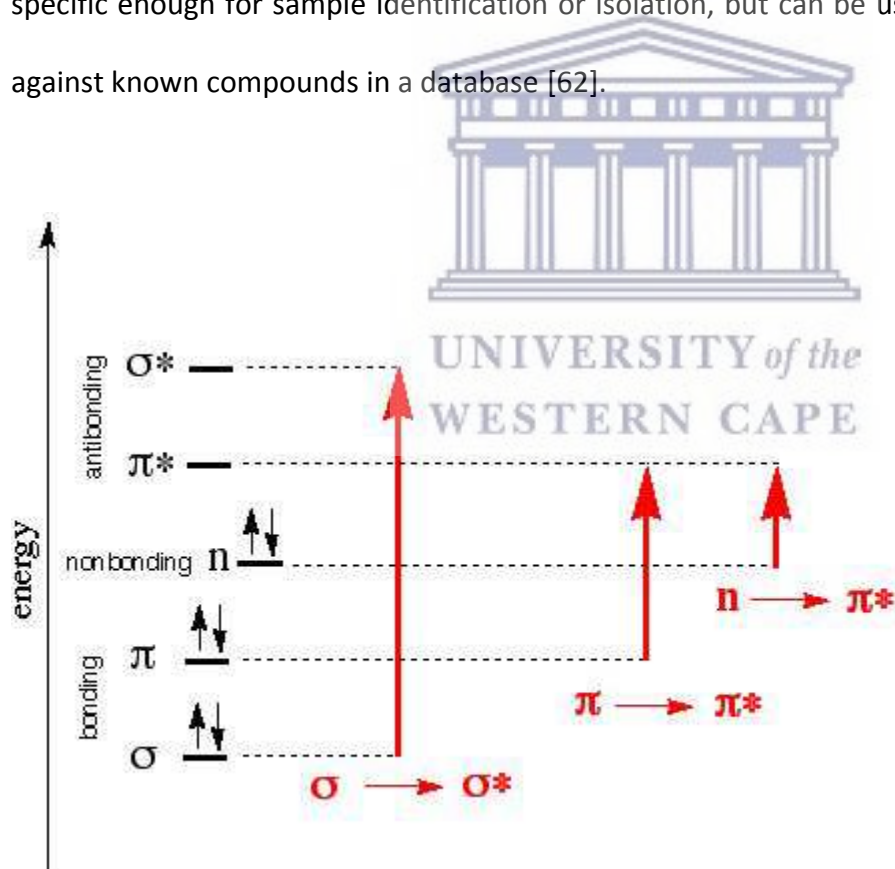


Figure 2-2: UV - VIS energy diagram [63].

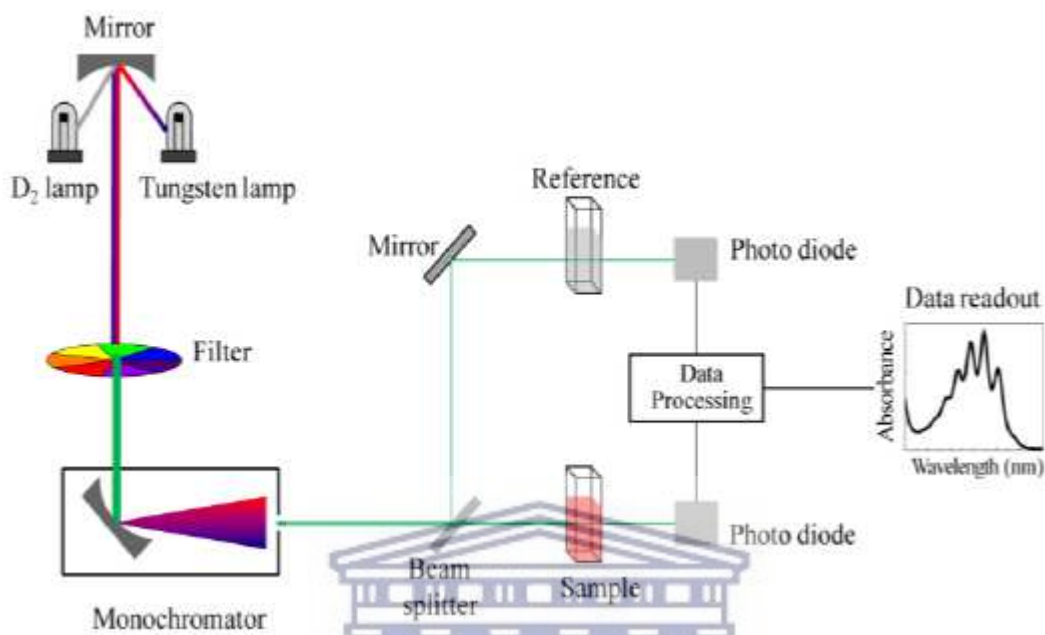


Figure 2-3: Diagram of a UV - VIS spectrometer [64].

2.3.3 Thermogravimetric analysis (TGA)

Thermogravimetric analysis (TGA) is a technique by which a sample weight is constantly checked while the sample is heated or cooled via a controlled temperature program and in a controlled atmosphere [65]. The TGA apparatus comprises a precision balance supported sample crucible located in a furnace that is heated and cooled during the testing. The sample's environment is controlled by an inert or reactive purge gas that is evacuated through the exhaust, while the mass of the sample is recorded constantly. TGA devices produce quantitative data relevant to loss of water, solvents, plasticizers, decomposition, decarboxylation and

weight percent filler among other. These data can be obtained by heating as well as cooling [65].

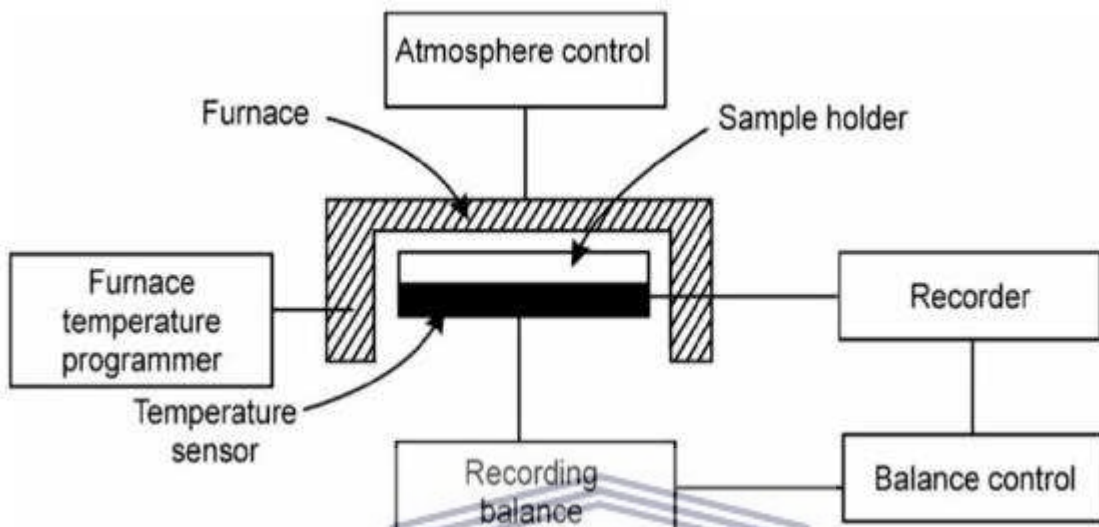


Figure 2-4: Diagram of a TGA machine [66].

UNIVERSITY of the
WESTERN CAPE

2.3.4 Nuclear magnetic resonance (NMR)

Nuclear magnetic resonance spectroscopy, commonly referred to as NMR, has become the preeminent technique for determining the structure of organic compounds over five decades. Of all the spectroscopic techniques, it is the only one for which a complete analysis and interpretation of the entire spectrum is normally expected. Although larger amounts of sample are needed than for mass spectroscopy, NMR is non-destructive, and with modern instruments good data may be obtained from samples weighing less than a milligram.

The ^1H NMR gives information about the chemical environment of a proton or group of protons relative tetramethylsilane (TMS). The ^{13}C NMR analysis is based on the same principles as the ^1H NMR technique, but the spectrum does not include any splitting. The ^{13}C NMR spectrum displays single peaks corresponding to each carbon environment or each set of equivalent carbon in the compound.

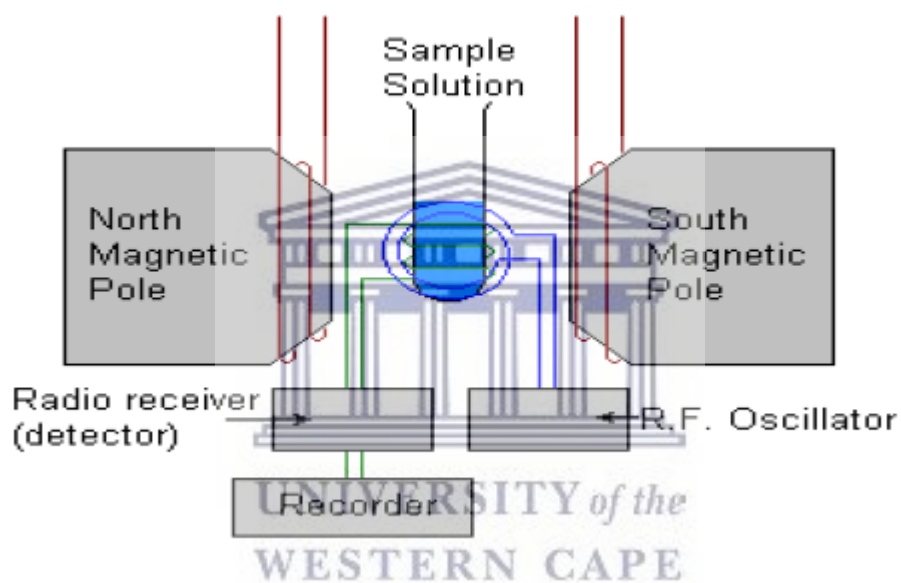
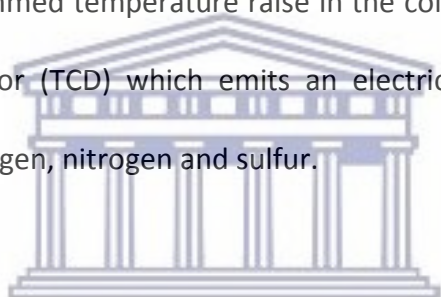


Figure 2-5: Diagram of NMR spectrometer [67].

2.3.5 Elemental analysis

Server 1112 Series Elemental Analyzer at the University of Stellenbosch central analytical facility was utilized to perform the carbon, hydrogen, and nitrogen and sulfur analysis. The

procedure involves weighing the samples into tin cups and loaded into an automatic sampler. The tin cups, required for the appropriate combustion in the elemental analyzer, travel down a tube where they undergo flash combustion at temperature of 1800°C. The gaseous combustion products N_2 , NO_x , H_2O , SO_2 , O_2 and CO_2 are carried by the helium as gas carrier through a column filled with copper oxide, and from there through a Cu column where nitrogen oxides are reduced to elementary nitrogen, and O_2 to CuO. Water is captured through another column and the remaining gases are passed through a temperature programmed desorption column (TPD) where N_2 is going straight through and the other gases are bound. The bound gases are released singly using a programmed temperature raise in the column. These gases travel along a thermal conductivity detector (TCD) which emits an electrical signal proportional to the concentration of carbon, Hydrogen, nitrogen and sulfur.



UNIVERSITY of the
WESTERN CAPE

2.4 Synthesis of Schiff base ligands

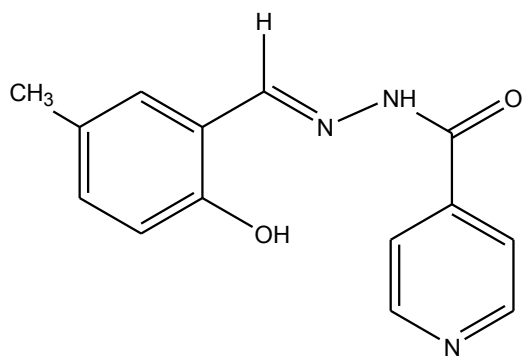
2.4.1 Isonicotinyl acid (2-hydroxy-5-methyl-benzilidene) – hydrazide (L1)

To a 15 mL methanolic solution of Isonicotinic acid hydrazide (INH) (1 mmol) in a schlenk tube, 15 mL solution of 2-Hydroxy-5-methyl-benzaldehyde (1 mmol) was added. To the light yellow solution magnesium sulfate (0.5 g) was added, which made the color turn yellow. The solution

was constantly under nitrogen and then stirred while under reflux for four hours. The reaction mixture was filtered to remove the magnesium sulfate after which the solvent was removed at the rotary evaporator to yield an off – white powder. This was recrystallized from 6 mL of methanol/diethyl ether (1:3), filtered and washed with diethyl ether and dried under reduced pressure. The pale white solid product was further dried for twenty four hours in a desiccator under vacuum.

The yield was 72%; the melting point was 235 °C – 237 °C. Infrared spectroscopy (cm^{-1}); ν (C=N) 1557. ^1H NMR (400 MHz CD_3OD): aromatic proton peaks δ 8.68 ppm (d, 1H), 7.80 ppm (s, 1H), 7.18 ppm (d, 1H), 7.07 ppm (d, 1H), 6.76 ppm (d, 1H); imine proton peak δ 7.82 ppm (s, 1H); hydrazine proton peak δ 8.43 ppm (s, 1H); hydroxyl proton peak δ 2.07 ppm (s, 1H). ^{13}C NMR (200 MHz, CD_3OD): aromatic peaks δ 149.90 ppm, 140.90 ppm, 132.64 ppm, 130.27 ppm, 128.55 ppm, 121.76 ppm, 117.61 ppm, 121.33 ppm, 116.19 ppm; amide carbon peak δ 162.37 ppm; imine peak δ 151.51 ppm. UV – VIS spectroscopy displayed a $\pi \rightarrow \pi^*$ transition at 215 nm and 244 nm and $n \rightarrow \pi^*$ transition at 292 nm and 344 nm. The lambda maximum was 215 nm.

Elemental analysis for $\text{C}_{14}\text{H}_{13}\text{N}_3\text{O}_2$ (255.27 g/mol), calculated: C, 65.87; H, 5.13; N, 16.46. Found: C, 64.57; H, 5.70; N, 16.19.



Isonicotinic acid
(2-hydroxy-5-methyl-benzylidene)-hydrazide

Figure 2-6: Structure of ligand L1

2.4.2 Isonicotinyl acid (2-hydroxy-5-methoxy-benzilidene)- hydrazide (L2)

To a 15 mL methanolic solution of Isonicotinic acid hydrazide (INH) (1 mmol) in a schlenk tube, 15 mL methanolic of 2-Hydroxy-5-methyl-benzaldehyde (1 mmol) was added. To the light orange solution magnesium sulfate (0.5 g) was added, which made the color turn orange. The solution was constantly under nitrogen and then stirred while under reflux for eight hours. The reaction mixture was filtered to remove the magnesium sulfate after which the solvent was removed at the rotary evaporator to yield yellow powder. This was recrystallized from 6 mL of methanol/diethyl ether (1:3), filtered and washed with diethyl ether and dried under reduced pressure. The yellow solid product was further dried for twenty four hours in a desiccator under vacuum.

The yield was 67%; the melting point was 241 °C – 243 °C. Infrared spectroscopy (cm^{-1}); ν (C=N) 1579. ^1H NMR (400 MHz CD_3OD): aromatic proton peaks δ 8.16 ppm (d, 1H), 8.14 ppm (d, 1H),

7.39 ppm (s, 1H), 7.18 ppm (d, 1H), 7.12 ppm (d, 1H); imine proton peak δ 8.81 ppm (s, 1H); hydrazine proton peak δ 9.00 ppm (s, 1H); hydroxyl proton peak δ 9.02 ppm (s, 1H). ^{13}C NMR (200 MHz, CD_3OD): aromatic peaks δ 150.50 ppm, 152.17 ppm, 149.74 ppm, 140.91 ppm, 121.77 ppm, 119.09 ppm, 118.21 ppm, 116.19 ppm, 112.65 ppm; amide peak δ 162.57 ppm; imine peak δ 149.74 ppm. UV – VIS spectroscopy displayed a π to π^* transition at 215 nm and n to π^* transition at 291 nm and 355 nm. The lambda maximum was 215 nm. Elemental analysis for $\text{C}_{14}\text{H}_{13}\text{N}_3\text{O}_3$ (271.27 g/mol), calculated: C, 61.99; H, 4.13; N, 15.49. Found: C, 62.92; H, 5.02; N, 15.64.

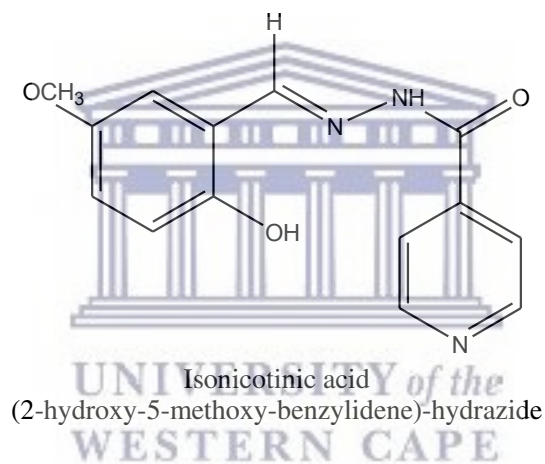


Figure 2-7: Structure of ligand L2

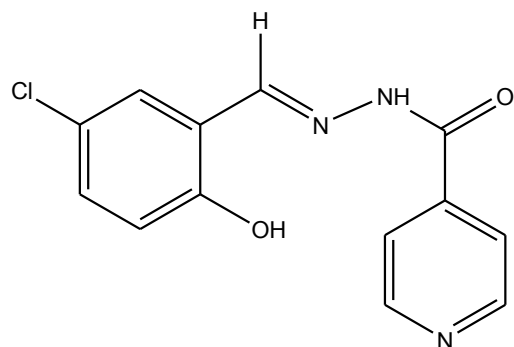
2.4.3 Isonicotinyl acid (5-chloro-2-hydroxy-benzilidene) – hydrazide (L3)

To a 15 mL methanolic solution of Isonicotinic acid hydrazide (INH) (1 mmol) in a schlenk tube was added 15 mL methanolic solution of 5-chloro-2-Hydroxy-benzaldehyde (1 mmol). To the yellowish solution magnesium sulfate (0.5 g) was added, which made the color turn pale yellow.

The solution was constantly under nitrogen and then stirred while under reflux for four hours.

The reaction mixture was filtered to remove the magnesium sulfate after which the solvent was removed at the rotary evaporator to yield an off – white powder. This was recrystallized from 6 mL of methanol/diethyl ether (1:3), filtered and washed with diethyl ether and dried under reduced pressure. The off - white solid product was further dried for twenty four hours in a desiccator under nitrogen.

The yield was 66%; the melting point was 246 °C – 248 °C. Infrared spectroscopy (cm^{-1}); ν (C=N) 1551. ^1H NMR (400 MHz CD_3OD): aromatic proton peaks δ 8.41 ppm (d, 1H), 7.78 ppm (d, 1H), 7.90 ppm (d, 1H), 7.70 ppm (d, 1H), 7.739 ppm (d, 1H); imine proton peak δ 8.31 ppm (s, 1H); hydrazine proton peak δ 8.89 ppm (s, 1H); hydroxyl proton peak δ 9.20 ppm (s, 1H). ^{13}C NMR (200 MHz, CD_3OD): aromatic carbon peaks δ 161.23 ppm, 149.68 ppm, 148.49 ppm, 140.30 ppm, 130.88 ppm, 129.05 ppm, 123.26 ppm, 121.33 ppm, 117.82 ppm; amide carbon peak δ 162.39 ppm; imine carbon peak δ 155.96 ppm. UV – VIS spectroscopy displayed a $\pi \rightarrow \pi^*$ transition at 221 nm and 248 nm and $n \rightarrow \pi^*$ transition at 289 nm and 343 nm. The lambda maximum was 221 nm. Elemental analysis for $\text{C}_{13}\text{H}_{10}\text{ClN}_3\text{O}_2$ (275.69 g/mol), calculated: C, 56.64; H, 3.66; N, 15.24. Found: C, 56.75; H, 3.73; N, 15.40. TGA studies displayed two stages of degradation that are 220 °C – 370 °C corresponding to a mass loss of 28.23 % ($\text{C}_2\text{H}_2\text{N}_2\text{O}$) and 370 °C – 700 °C leading to a mass loss of 62.67 % ($\text{C}_5\text{H}_5\text{N}$).



Isonicotinic acid
(5-chloro-2-hydroxy-benzylidene)-hydrazide

Figure 2-8: Structure of ligand L3

2.4.4 Isonicotinyl acid (5-bromo-2-hydroxy-benzilidene) – hydrazide (L4)

To a 15 mL methanolic solution of Isonicotinic acid hydrazide (INH) (1 mmol) in a schlenk tube was added 15 methanolic solution of 5-bromo-2-Hydroxy-benzaldehyde (1 mmol). To the clear solution magnesium sulfate (0.5 g) was added, which made the color turn whitish. The solution was constantly under nitrogen and then stirred while under reflux for four hours. The reaction mixture was filtered to remove the magnesium sulfate after which the solvent was removed at the rotary evaporator to yield a bright – white powder. This was recrystallized from 6 mL of methanol/diethyl ether (1:3), filtered and washed with diethyl ether and dried under reduced pressure. The bright white solid product was further dried for twenty four hours in a desiccator under vacuum.

The yield was 65%; the melting point was 259 °C – 261 °C. Infrared spectroscopy (cm^{-1}); ν (C=N) 1550. ^1H NMR (400 MHz CD_3OD): aromatic proton peaks δ 7.83 ppm (d, 1H), 7.56 ppm (d, 1H),

7.31 ppm (d, 1H), 6.71 ppm (d, 1H), 6.69 ppm (d, 1H); imine proton peak δ 8.65 ppm (s, 1H); hydrazine proton peak δ 8.67 ppm (s, 1H); hydroxyl proton peak δ 10.15 ppm (s, 1H). ^{13}C NMR (200 MHz, CD_3OD): aromatic carbon peaks δ 149.94 ppm, 148.93 ppm, 133.55 ppm, 121.82 ppm, 119.92 ppm, 113.43 ppm, 113.31 ppm, 121.33 ppm, 117.82 ppm; amide carbon peak δ 157.20 ppm; imine carbon peak δ 149.74 ppm. UV – VIS spectroscopy displayed a $\pi \rightarrow \pi^*$ transition at 225 nm and $n \rightarrow \pi^*$ transition at 292 nm and 346 nm. The lambda maximum was 225 nm. Elemental analysis for $\text{C}_{13}\text{H}_{10}\text{BrN}_3\text{O}_2$ (320.14 g/mol), calculated: C, 48.77; H, 3.15; N, 13.13. Found: C, 48.76; H, 3.04; N, 13.22. TGA studies displayed 2 stages of decomposition that are 320 °C – 370 °C corresponding to a mass loss of 26.6 % ($\text{C}_2\text{H}_2\text{N}_2\text{O}$) and 370 °C – 700 °C leading to a mass loss of 62.4 % ($\text{C}_5\text{H}_5\text{N}$).

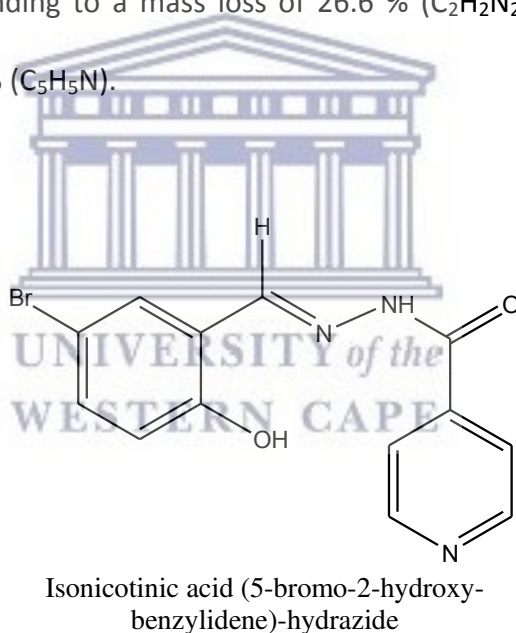


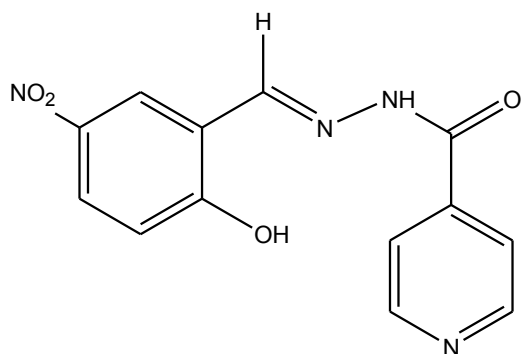
Figure 2-9: Structure of ligand L4

2.4.5 Isonicotinyl acid (2-hydroxy-5-nitro-benzilidene) – hydrazide (L5)

To a 15 mL methanolic solution of Isonicotinic acid hydrazide (INH) (1 mmol) in a schlenk tube was added 15 mL methanolic solution of 2-Hydroxy-5-nitro-benzaldehyde (1 mmol). To the light orange solution magnesium sulfate (0.5 g) was added, which made the color turn bright orange. The solution was constantly under nitrogen and then stirred while under reflux for four hours. The reaction mixture was filtered to remove the magnesium sulfate after which the solvent was removed at the rotary evaporator to yield a bright orange powder. This was recrystallized from 6 mL of methanol/diethyl ether (1:3), filtered and washed with diethyl ether and dried under reduced pressure. The bright orange solid product was further dried for twenty four hours in a desiccator under vacuum.

The yield was 59%; the melting point was 269 °C – 271 °C. Infrared spectroscopy (cm^{-1}); ν (C=N) 1546. ^1H NMR (400 MHz DMSO D_6): aromatic proton peaks δ 8.87 ppm (d, 1H), 8.68 ppm (d, 1H), 8.26 ppm (d, 1H), 7.92 ppm (d, 1H), 7.70 ppm (d, 1H); imine proton peak δ 8.83 ppm (s, 1H); hydrazine proton peak δ 8.86 ppm (s, 1H); hydroxyl proton peak δ 7.19 ppm (s, 1H). ^{13}C NMR (200 MHz, DMSO D_6): aromatic carbon peaks δ 161.78 ppm, 145.38 ppm, 140.34 ppm, 127.14 ppm, 123.96 ppm, 122.54 ppm, 121.79 ppm, 120.38 ppm, 117.20 ppm; amide carbon peak δ 163.22 ppm; imine carbon peak δ 151.07 ppm. UV – VIS spectroscopy displayed a $\pi \rightarrow \pi^*$ transition at 210 nm and $\eta \rightarrow \pi^*$ transition at 288 nm and at 324 nm. The lambda maximum was displayed at 210 nm. . Elemental analysis for $\text{C}_{13}\text{H}_{10}\text{N}_4\text{O}_2$ (286.24 g/mol), calculated: C, 54.55; H, 3.52; N, 19.57. Found: C, 54.19; H, 3.37; N, 19.43. TGA studies displayed 2 stages that

are 320 °C – 370 °C corresponding to a mass loss of 27.67 % (C₂H₂N₂O) and 370 °C – 700 °C leading to a mass loss of 62.33 % (C₅H₄N).



Isonicotinic acid
(2-hydroxy-5-nitro-benzylidene)-hydrazide

Figure 2-10: Structure for ligand L5

2.5 Ruthenium complexes of the Schiff base ligands

2.5.1 General remarks

Complexation in coordination chemistry refers to a central atom or ion, usually a transition metal in the periodic table, bonded or coordinated to a surrounding array of molecules or ions. The central atom is designated as the coordination center, while the surrounding array of molecules or ions is called ligands or complexing agents.

A known amount of the ruthenium precursor $\text{RuCl}_2(\text{DMSO})_4$ is dissolved in 10 mL of freshly distilled ethanol in a schlenk tube under inert atmosphere. An equimolar mixture of the ligand and the metal complex precursor in freshly distilled ethanol was refluxed under inert atmosphere at 60°C for four hours. Upon completion the excess solvent is removed under vacuum and the solid product is collected post filtration using a 1:3 ratio of solvent mixture of ethanol/diethyl ether and washed with excess diethyl ether.

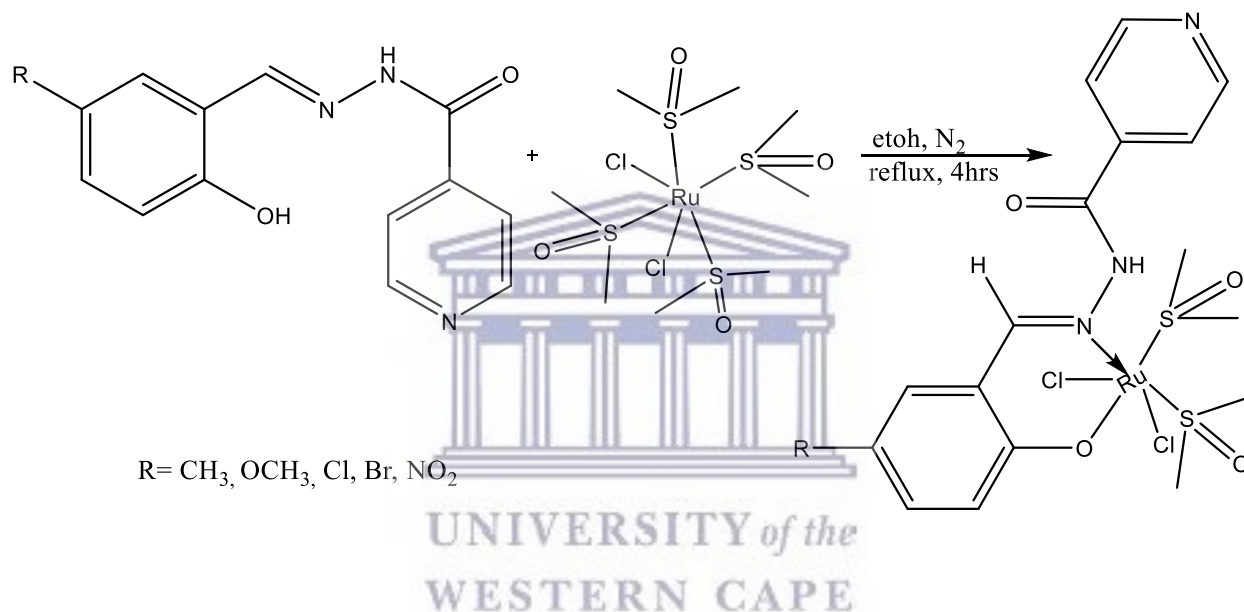


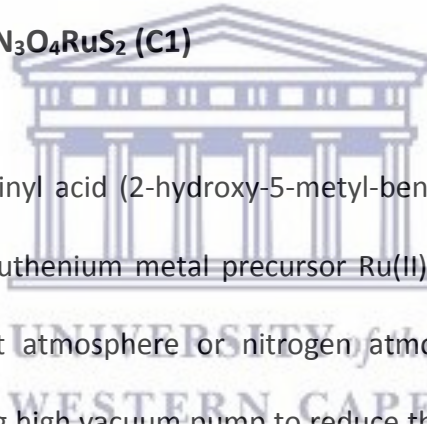
Figure 2-11: Scheme of isoniazid Schiff base complex

2.5.2 Synthesis of the Ruthenium precursor $\text{RuCl}_2(\text{DMSO})_4$

The ruthenium (II) precursor $\text{RuCl}_2(\text{DMSO})_4$ was synthesized by dissolving 2g of $\text{RuCl}_3 \cdot x\text{H}_2\text{O}$ in 50 mL of ethanol according to literature procedure [17]. The reaction was refluxed for 3 hours under nitrogen, using general schlenk techniques. During the reaction a color change is

observed from black to dark green. After the allotted time any unreactive materials is filtered off. The solvent is removed on a rotary evaporator, and thick green oil is observed. 9 mL DMSO is added to the reaction mixture and refluxed for another 2 hours or more until yellow solids is observed. This is followed by the addition of 60 mL acetone and stored in the fridge overnight. The solvent was removed under reduced pressure using liquid nitrogen and a yellow crystalline powder was collected.

2.5.3 Synthesis of $C_{18}H_{26}Cl_2N_3O_4RuS_2$ (C1)



The Schiff base ligand Isonicotinyl acid (2-hydroxy-5-methyl-benzilidene) – hydrazide (1 mmol) was taken together with the ruthenium metal precursor $Ru(II)Cl_2(DMSO)_4$ (1 mmol) in 20 mL ethanolic solution under inert atmosphere or nitrogen atmosphere for four hours whilst refluxing. Solvent removal using high vacuum pump to reduce the methanol amount to about 2 mL took place after the four hour reflux, then the addition of excess amount for diethyl ether was done to cause the product to precipitate and to wash the product. A cannula was used to transfer out the remaining small volume of methanol/ diethyl ether from the reaction vessel. The dried product color was light brown and the yield amount was 69 percent. The melting point was 248 °C – 250 °C. Infrared spectroscopy (cm^{-1}); ν (C=N) 1541. 1H NMR (400 MHz CD_3OD): aromatic proton peaks δ 8.19 ppm (d, 1H), 8.14 ppm (d, 1H), 7.97 ppm (s, 1H), 7.85 ppm (d, 1H), 7.44 ppm (d, 1H), 6.89 ppm (d, 1H); imine proton peak δ 8.00 ppm (s, 1H);

hydrazine proton peak δ 8.91 ppm (s, 1H); methyl proton peak δ 2.31 ppm (s, 1H), dimethyl proton peak δ 3.48 ppm (s, 12H). UV – VIS spectroscopy displayed a $\pi \rightarrow \pi^*$ transition at 203 nm and $\eta \rightarrow \pi^*$ transition at 292 nm and 349 nm. The lambda maximum was 203 nm. Elemental analysis for $C_{18}H_{26}Cl_2N_3O_4RuS_2$ (584.52 g/mol), calculated: C, 37.11; H, 4.15; N, 7.21; S, 11.01. Found: C, 36.99; H, 4.45; N, 6.61; S, 11.76.

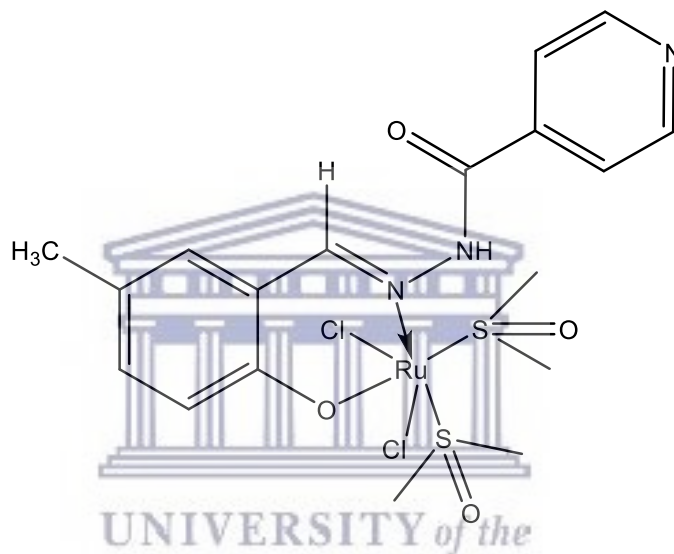
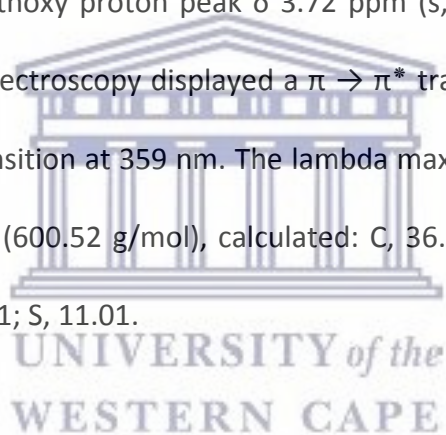


Figure 2-12: Structure of complex C1

2.5.4 Synthesis of $C_{18}H_{26}Cl_2N_3O_5RuS_2$ (C2)

The Schiff base ligand Isonicotinyl acid (2-hydroxy-5-methoxy-benzilidene) – hydrazide (1 mmol) was taken together with the ruthenium metal precursor $Ru(II)Cl_2(DMSO)_4$ (1 mmol) in 20 mL methanolic solution under inert atmosphere or nitrogen atmosphere for four hours whilst

refluxing. Solvent removal using high vacuum pump to reduce the methanol amount to about 2 mL took place after the four hour reflux, then the addition of excess amount for diethyl ether was done to cause the product to precipitate and to wash the product. A cannula was used to transfer out the remaining small volume of methanol/ diethyl ether from the reaction vessel. The dried product color was brittle-dark brown and the yield amount was 67 percent. The melting point was 258 °C – 260 °C. Infrared spectroscopy (cm^{-1}); ν (C=N) 1570. ^1H NMR (400 MHz CD_3OD): aromatic proton peaks δ 8.14 ppm (d, 1H), 7.80 ppm (s, 1H), 7.13 ppm (d, 1H), 6.97 ppm (d, 1H), 6.88 ppm (d, 1H); imine proton peak δ 7.94 ppm (s, 1H); hydrazine proton peak δ 10.25 ppm (s, 1H); methoxy proton peak δ 3.72 ppm (s, 1H), dimethyl proton peak δ 3.56 ppm (s, 12H). UV – VIS spectroscopy displayed a $\pi \rightarrow \pi^*$ transition at 204 nm, at 226 nm and at 256 nm and $\eta \rightarrow \pi^*$ transition at 359 nm. The lambda maximum was 204 nm. Elemental analysis for $\text{C}_{18}\text{H}_{26}\text{Cl}_2\text{N}_3\text{O}_5\text{RuS}_2$ (600.52 g/mol), calculated: C, 36.12; H, 4.04; N, 7.02; S, 10.72. Found: C, 35.49; H, 4.45; N, 6.61; S, 11.01.



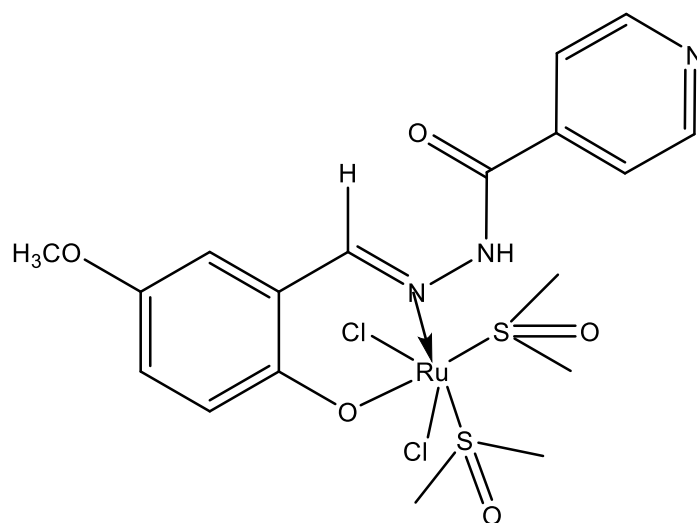


Figure 2-13: Structure of complex C2



2.5.5 Synthesis of $C_{17}H_{23}Cl_3N_3O_4RuS_2$ (C3)

UNIVERSITY of the
WESTERN CAPE

The Schiff base ligand Isonicotinyl acid (5-chloro-2-hydroxy-benzilidene) – hydrazide (1 mmol) was taken together with the ruthenium metal precursor $Ru(II)Cl_2(DMSO)_4$ (1 mmol) in 20 mL ethanolic solution under inert atmosphere or nitrogen atmosphere for four hours whilst refluxing. Solvent removal using high vacuum pump to reduce the ethanol amount to about 2 mL took place after the four hour reflux, then the addition of excess amount for diethyl ether was done to cause the product to precipitate and to wash the product. A cannula was used to transfer out the remaining small volume of ethanol/ diethyl ether from the reaction vessel. The dried product color was pale brown and the yield amount was 65 percent.

The melting point was 263 °C – 265 °C. Infrared spectroscopy (cm^{-1}); ν (C=N) 1543. ^1H NMR (400 MHz CD_3OD): aromatic proton peaks δ 8.02 ppm (d, 1H), 7.97 ppm (s, 1H), 7.72 ppm (d, 1H), 7.59 ppm (d, 1H), 7.07 ppm (d, 1H); imine proton peak δ 7.82 ppm (s, 1H); hydrazine proton peak δ 8.83 ppm (s, 1H); methyl proton peak δ 3.20 ppm (s, 1H). UV – VIS spectroscopy displayed a $\pi \rightarrow \pi^*$ transition at 203 nm and 219 nm and $\eta \rightarrow \pi^*$ transition at 288 nm and 345 nm. The lambda maximum was 203 nm. Elemental analysis for $\text{C}_{17}\text{H}_{23}\text{Cl}_3\text{N}_3\text{O}_4\text{RuS}_2$ (604.94 g/mol), calculated: C, 33.87; H, 3.51; N, 6.97; S, 10.64. Found: C, 33.49; H, 4.45; N, 6.61; S, 11.01. The TGA studies display three stages of decomposition that are 75 °C – 250 °C corresponding to a loss of 2.3 % (H_2O), then 250 °C – 370 °C corresponding to a loss of 9.5 % (Cl_2) and 370 °C – 700 °C leading to a loss of 59 % ($\text{C}_4\text{H}_{14}\text{Cl}_2\text{O}_3\text{RuS}_2$).

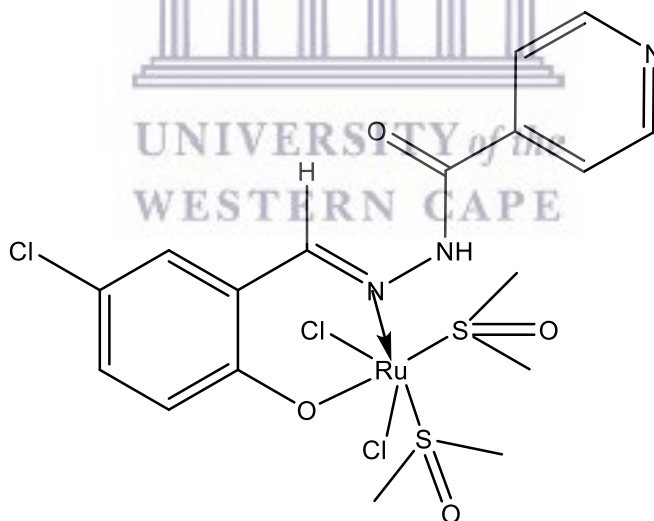


Figure 2-14: Structure for complex C3

2.5.6 Synthesis of $C_{17}H_{23}BrCl_2N_3O_4RuS_2$ (C4)

The Schiff base ligand Isonicotinyl acid (5-bromo-2-hydroxy-benzilidene) – hydrazide (1 mmol) was taken together with the ruthenium metal precursor $Ru(II)Cl_2(DMSO)_4$ (1 mmol) in 20 mL methanolic solution under inert atmosphere or nitrogen atmosphere for four hours whilst refluxing. Solvent removal using high vacuum pump to reduce the methanol amount to about 2 mL took place after the four hour reflux, then the addition of excess amount for diethyl ether was done to cause the product to precipitate and to wash the product. A cannula was used to transfer out the remaining small volume of methanol/ diethyl ether from the reaction vessel. The dried product color was pale brown and the yield amount was 66 percent.

The melting point was 268 °C – 270 °C. Infrared spectroscopy (cm^{-1}); ν (C=N) 1547. 1H NMR (400 MHz CD_3OD): aromatic proton peaks δ 8.65 ppm (d, 1H), 7.94 ppm (d, 1H), 7.84 ppm (s, 1H), 7.72 ppm (d, 1H), 6.93 ppm (d, 1H); imine proton peak δ 7.98 ppm (s, 1H); hydrazine proton peak δ 8.83 ppm (s, 1H); methyl proton peak δ 3.19 ppm (s, 1H). UV – VIS spectroscopy displayed a π to π^* transition at 205 nm and 218 nm and n to π^* transition at 291 nm and 348 nm. The lambda maximum was 205 nm. Elemental analysis for $C_{17}H_{23}BrCl_2N_3O_4RuS_2$ (649.39 g/mol), calculated: C, 31.54; H, 3.21; N, 6.49; S, 9.91. Found: C, 30.67; H, 4.17; N, 6.61; S, 10.51. The TGA studies display three stages of decomposition that are 75 °C – 250 °C corresponding to a loss of 5.7 % (H_2O), then 250 °C – 370 °C corresponding to a loss of 12.86 % (Cl_2) and 370 °C – 700 °C leading to a loss of 66 % ($C_4H_{14}Cl_2O_3RuS_2$).

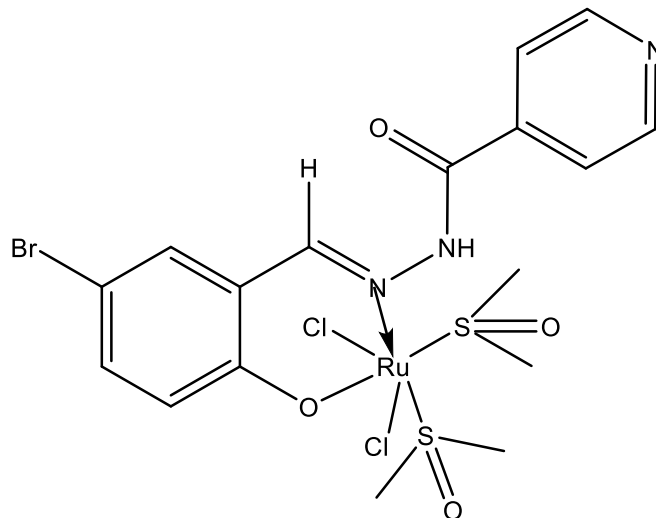


Figure 2-15: Structure for complex C4



2.5.7 Synthesis of $C_{17}H_{23}Cl_2N_4O_6RuS_2$ (C5)

The Schiff base ligand isonicotinyl acid (2-hydroxy-5-nitro-benzilidene) – hydrazide (1 mmol) was taken together with the ruthenium metal precursor $Ru(II)Cl_2(DMSO)_4$ (1 mmol) in 20 mL methanolic solution under inert atmosphere or nitrogen atmosphere for four hours whilst refluxing. Solvent removal using high vacuum pump to reduce the methanol amount to about 2 mL took place after the four hour reflux, then the addition of excess amount for diethyl ether was done to cause the product to crash out and to wash the product. A cannula was used to transfer out the remaining small volume of methanol/ diethyl ether from the reaction vessel. The dried product color was light brown and the yield amount was 73 percent. The melting point was 276 °C – 278 °C. Infrared spectroscopy (cm^{-1}); ν (C=N) 1540. 1H NMR (400 MHz

CD₃OD): aromatic proton peaks δ 8.16 ppm (d, 1H), 8.89 ppm (d, 1H), 7.99 ppm (s, 1H), 7.96 ppm (d, 1H), 7.19 ppm (d, 1H); imine proton peak δ 8.81 ppm (s, 1H); hydrazine proton peak δ 8.84 ppm (s, 1H); methyl proton peak δ 2.50 ppm (s, 1H). UV – VIS spectroscopy displayed a $\pi \rightarrow \pi^*$ transition at 205 nm and $\eta \rightarrow \pi^*$ transition at 333 nm and at 405 nm. The lambda maximum was displayed at 205 nm. Elemental analysis for C₁₇H₂₃Cl₂N₄O₆RuS₂ (615.49 g/mol), calculated: C, 33.28; H, 3.45; N, 9.13; S, 10.45. Found: C, 32.45; H, 4.17; N, 9.65; S, 9.58. The TGA studies display three stages of decomposition that are 75 °C – 250 °C corresponding to a loss of 4.1 % (H₂O), then 250 °C – 320 °C corresponding to a loss of 33.33 % (C₁₃H₉N₃O) and 320 °C – 700 °C leading to a loss of 66 % (C₄H₁₄Cl₂O₃RuS₂).

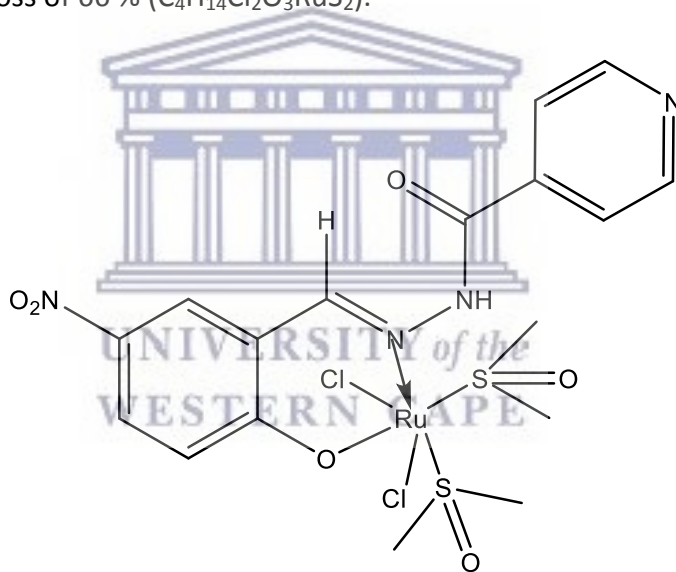


Figure 2-16: Structure of complex C5

Chapter 3: Results and discussion

3.1 Schiff base ligands

3.1.1 General remarks

A Schiff base is a nitrogen analog of an aldehyde or ketone involving the replacement of the C=O group by C=N-R group. They are the products of condensation reaction of ketones or aldehydes with primary amines [53].

Schiff bases that have aryl substituents are much more stable and more easily synthesized, while those which contain alkyl substituents are somewhat unstable. Schiff bases of aliphatic aldehydes are generally unstable and easily polymerizable while those of aromatic aldehydes having effective conjugation are more stable. The formation is generally driven to the completion by separation of the product or removal of water, or both. Many Schiff bases can be hydrolyzed back to their aldehydes or ketones and amines by aqueous acid or base.



Figure 3-1: Scheme of Schiff base ligand synthesis

The mechanism of Schiff base formation is another variation on the theme of nucleophilic addition to the carbonyl group. In this case, the nucleophile is the amine. In the first part of the mechanism, the amine reacts with the aldehyde or ketone to give an unstable addition compound called carbinolamine. The carbinolamine loses water by either acid or base catalyzed pathways. Since the carbinolamine is an alcohol, it undergoes acid catalyzed dehydration.

Typically the dehydration of the carbinolamine is the rate-determining step of Schiff base formation and that is why the reaction is catalyzed by acids. Yet the acid concentration can't be too high because amines are basic compounds. If the amine is protonated and becomes non-nucleophilic, equilibrium is pulled to the left and carbinolamine formation can't occur. Therefore, many Schiff bases synthesis are best carried out at mildly acidic pH. The dehydration of carbinolamines is also catalyzed by base. This reaction is somewhat analogous to the E2 elimination of alkyl halides except that it is not a concerted reaction. It proceeds in two steps through an anionic intermediate. The Schiff base formation is really a sequence of two types of reactions, i.e. addition followed by elimination.

3.1.2 Ligands

All the synthesized ligands can be categorized as hydrazones, which is a class of ligands characterized by the functional group (C=N-N), that makes up a sub – group of the imine or Schiff base ligands [51]. All these ligands, having different substituents on the metha position, were synthesized following the same procedure of condensation reaction according to

literature (scheme 3) [54]. The substituents range from activating to deactivating. The alkyl functional group (CH₃) is activating as well as the methoxy group (OCH₃) with the remaining three other functional groups, namely the chlorine (Cl), the bromine (Br) and the nitro group (NO₂), being deactivating.

In this study project we report the synthesis and characterization of isoniazid Schiff base ligands, which we are hoping to be stable and active against microbes by themselves and upon coordination with ruthenium (II) transition metal in comparison to literature reports.

A one to one ratio of the primary amine isoniazid (INH) and one of the five aldehyde carrying different substituents were taken together in a methanolic solution under reflux for four hours (scheme 3) [51]. The monitoring of the reaction by FT - IR at two hours intervals indicated the disappearance of the starting materials and the appearance of the imine peak at the fourth hour of the preparation. The color of the ligands obtained were light yellow for **L1**, light orange for **L2**, off – white for **L3**, bright white for **L4**, and bright orange for **L5** respectively. The yields for the ligands were seventy two percent for **L1**, sixty seven percent for **L2**, sixty six percent for **L3**, sixty five percent for **L4**, and fifty nine percent for **L5**. All the ligands were stable at room temperature. They were slightly soluble in organic solvent such as methanol, ethanol, dichloromethane and water; but readily soluble in DMSO. Upon synthesis completion, all the ligands were subjected to FT – IR studies, UV – VIS studies, NMR studies as well as elemental analysis.

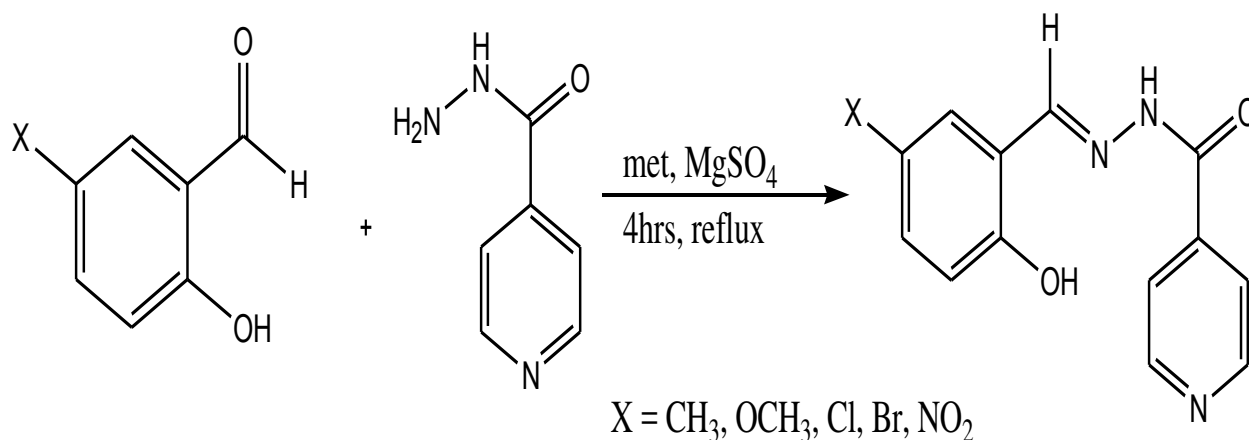


Figure 3-2: Schiff base ligand synthesis

3.1.2.1 Fourier transform infrared studies

The Fourier transform infrared spectrum confirmed the successful completion of the reaction by displaying the appearance of the azomethine or imine peak and the disappearance of the aldehyde functional group. Overall the ligands exhibited infrared spectroscopic features that were very similar. The spectral range for the measurement of the infrared spectra of the compounds was from four hundred to four thousand cm^{-1} . These FT – IR measurements were recorded in solid state using potassium bromide pellets. The functional groups of interest are the imine (C=N), the aldehyde carbonyl (HC=O) and amide carbonyl (NHC=O). The following spectrum of ligand **L1** (figure 3-3) is an example of the spectra for the prepared Schiff base ligands. The rest of ligand spectra **L2**, **L3**, **L4** and **L5** are ascribed in the appendix section. Table

3.1 below lists the frequencies of the functional groups that confirm the successful preparation of all the ligands.

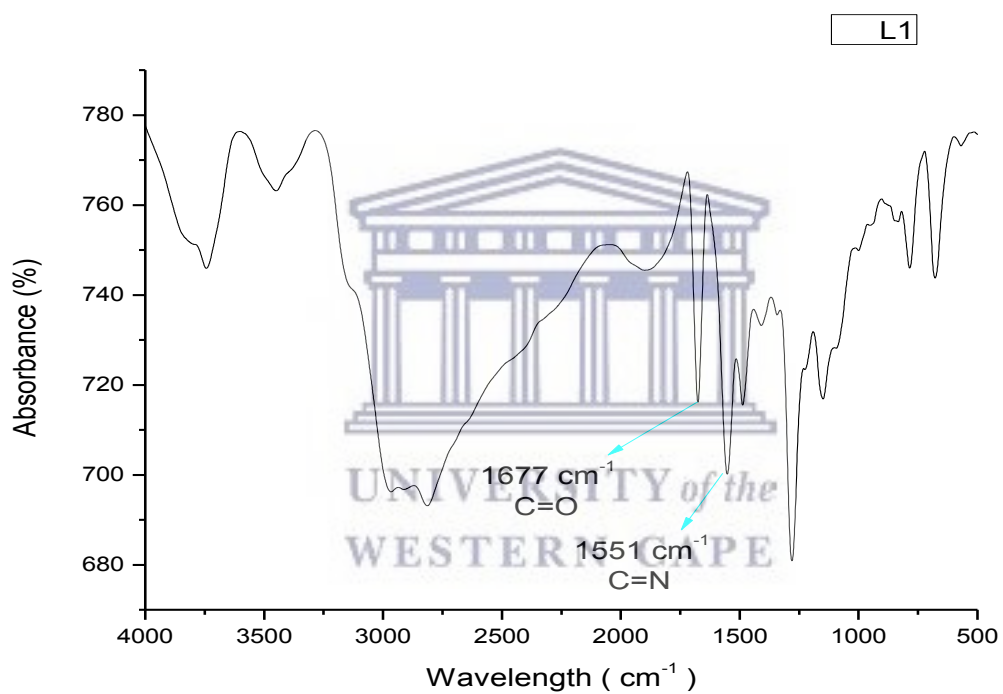
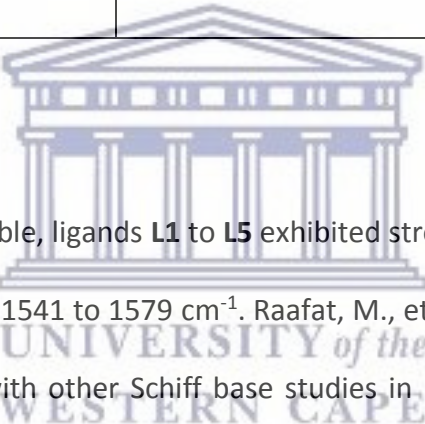


Figure 3-3: FTIR spectrum of ligand L1

Table 3-1: FTIR data, yield and color of ligands

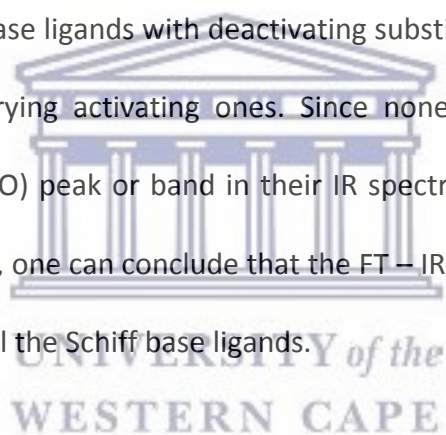
Ligands	FT – IR (cm ⁻¹)		% Yield	Color
	C=O	C=N		
L1	1673	1551	72	Light yellow
L2	1666	1579	67	Light orange
L3	1677	1551	66	Off - white
L4	1677	1541	65	Bright white
L5	1667	1551	59	Bright orange



In accordance with the above table, ligands **L1** to **L5** exhibited strong bands for the imine $\nu(\text{C}=\text{N})$ at the frequencies ranging from 1541 to 1579 cm^{-1} . Raafat, M., et al reported similar imine peak values that are in agreement with other Schiff base studies in literature [68]. However these frequencies displayed by all of the ligands are somewhat lower than the range reported by the majority of studies [51, 52, 69]. Ligands **L1**, **L3** and **L5** have the same frequency for the imine peak which is 1551 cm^{-1} . This fact is somewhat unusual since **L1** has an activating substituent the methyl group (CH_3) while **L3** and **L5** have deactivating substituents that are the Chlorine (Cl) and the nitro group (NO_2) respectively. The expected results should have been different frequencies for the ligands according to the type of substituents attached, whether they were activating or deactivating. Further analysis of the $\nu(\text{C}=\text{N})$ frequencies indicates that the methoxy substituted ligand L2 has the highest azomethine peak frequency 1579 cm^{-1} . These results of

the $\nu(\text{C}=\text{N})$ frequency values in the table can lead to deduce that activating substituents yield higher imine peak frequencies for Schiff base ligands than deactivating substituents do.

Looking at the values of the frequencies of the carbonyl $\nu(\text{C}=\text{O})$ for all ligands, it is noticeable the ligands **L3**, **L4** and **L5**, that are all carrying deactivating substituents namely chlorine (Cl), bromine (Br) and nitro (NO_2) respectively, yield higher frequencies for this functional group ($\text{C}=\text{O}$) than the ligands carrying activating ones **L1** (CH_3) and **L2** (OCH_3). Ligands **L3**, **L4** and **L5** strikingly display the same frequency of 1677 cm^{-1} for $\nu(\text{C}=\text{O})$ while **L1** and **L2** have lower but different $\nu(\text{C}=\text{O})$ frequencies of 1673 and 1666 cm^{-1} respectively. In light of this, the trend that can be deduced is that Schiff base ligands with deactivating substituent bare higher frequencies for $\nu(\text{C}=\text{O})$ than the ones carrying activating ones. Since none of the ligands displayed an aldehyde functional group (CHO) peak or band in their IR spectrum and all of them displayed strong band for the imine peak, one can conclude that the FT – IR spectra of the ligands confirm the successful preparation of all the Schiff base ligands.



3.1.2.2 Ultraviolet visible studies

UV – Vis absorption spectra of the ligands **L1** to **L5** were acquired using 1 cm micro cuvettes in methanol solvent at room temperature in the wavelength range of 200 to 800 nm. The electronic transitions occurring within the prepared compounds are depicted in the spectra. The following spectrum (figure 3-4) is a representative sample of the spectra obtained for Schiff

base ligands **L1** to **L5**. A summary of all electronic transitions is displayed in table 3.2 and the remaining spectra of ligands **L2** to **L4** are located in the appendix section.

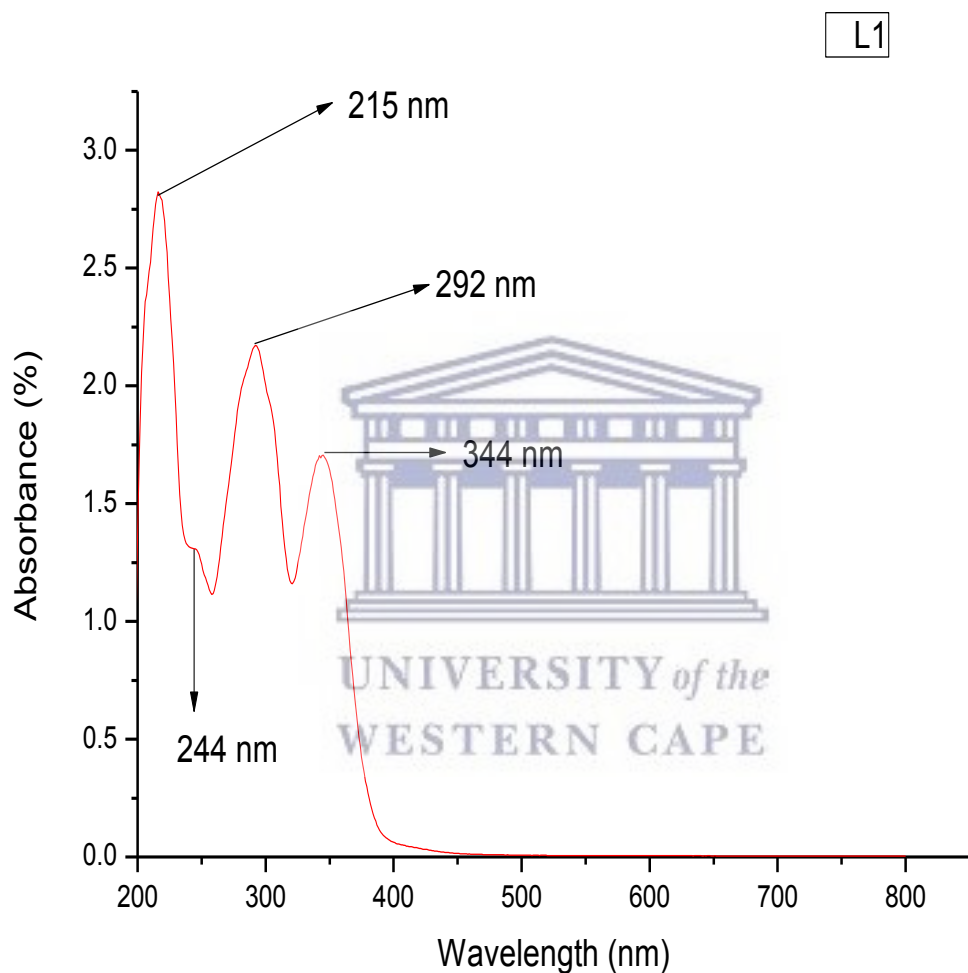


Figure 3-4: UV - VIS spectrum of ligand L1

Table 3-2: UV - VIS data of ligands

Ligands	Electronic transitions (nm)		
	$\pi \rightarrow \pi^*$	$n \rightarrow \pi^*$	λ_{max}
L1	215, 244, 292	344	215
L2	215, 291	355	215
L3	219, 249, 290	343	219
L4	203, 218, 250, 291	350	203
L5	210, 288	324	210

UNIVERSITY of the
WESTERN CAPE

The prepared Schiff ligands in this study are exhibiting electronic transitions in the range of 203 nm to 355 nm. All the ligands **L1** to **L5** display three to five absorption bands corresponding to two kinds of electronic transitions namely $\pi \rightarrow \pi^*$ and $n \rightarrow \pi^*$. The bands on the higher energy region from 203 nm to 292 nm are attributed to the excitation of the π electrons ($\pi \rightarrow \pi^*$ transitions) of the aromatic rings and the bands on the lower energy side ranging from 324 nm to 355 nm are assigned to the $n \rightarrow \pi^*$ transitions of the imine or azomethine functional group

(C=N) [68]. Hussain *et al* reported similar absorption bands in his study about Schiff bases of sulfamethoxazole [70].

3.1.2.3 Thermogravimetric analysis studies (TGA)

The TGA studies were only conducted for three ligands and their respective ruthenium (II) complexes. Those ligands are **L3**, **L4** and **L5** and their complexes are **C1**, **C2** and **C3**. The TGA studies were conducted in order to test the stability of the prepared compounds.



3.1.2.3.1 TGA of Schiff base ligands

To the best of our knowledge, the TGA studies of ligands **L3 to L5** and their respective complexes **C3 to C5** are being reported for the first time. Figure 3-5 of the graph of ligand **L3** below is a representative example of the TGA graph of all ligands. The remaining ligands graphs are located in the appendix section. Likewise the table 3.3 displays the decomposition points of all ligands studied with this technique. The TGA controlled temperature rate for the tested ligands was 10 °C per minute.

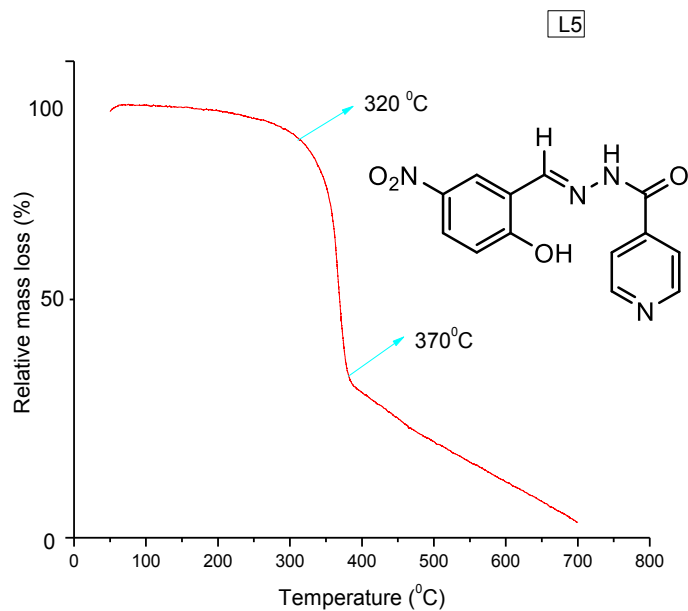


Figure 3-5: TGA graph of Ligand L5

UNIVERSITY of the
WESTERN CAPE
Table 3-3: TGA data for ligands

Ligands	Temperature range (°C)	Mass Loss % Calc/Found	Assignments
L 3	220 – 370	28.23 (29.11)	C ₂ H ₂ N ₂ O
	370 – 700	62.67 (61.93)	C ₅ H ₅ N
L 4	320 - 370	26.60 (27.530)	C ₂ H ₂ N ₂ O
	370 – 700	62.40 (63.24)	C ₅ H ₅ N
L 5	320 – 370	27.67 (26.98)	C ₂ H ₂ N ₂ O
	370 - 700	62.33 (63.12)	C ₅ H ₄ N

The thermogravimetric analysis table tells us the ligands **L3**, **L4** and **L5** start decomposing at 220 °C for **L3** and 320 °C for **L4** and **L5**. All tested ligands display 2 stages of decomposition. Figure 3-5 exhibits clearly the stages of decomposition of ligand **L5** and that **L5** is stable from 50 °C to 320 °C. The same trend is observed in ligands **L4** and **L5**. The first decomposition stage of **L3** of 320 °C – 370 °C corresponds to a mass loss of 26.98 % ($C_2H_2N_2O$) and the second one of 370 °C – 700 °C relates to a loss of 63.12 % (C_5H_5N). The calculated relative mass for stage one of **L5** is 26.98 % and for the second one is 63.12 %. Raziye A. et al. reported similar findings in his study about thermal studies of Cu (II) and Co (II) complexes with Schiff base dye ligands [71]. The decomposition stages of **L3** and **L4** are explicitly displayed in table 3-3.



3.1.2.4 Nuclear magnetic resonance studies

UNIVERSITY of the
WESTERN CAPE

In order to elucidate the structure of all five synthesized ligands **L1** – **L5**, proton (1H) and carbon NMR (^{13}C) were used for this endeavor. The deuterated solvents deemed suitable to do the NMR characterization are deuterated methanol and dimethyl sulfoxide at room temperature using trimethyl silane (TMS) as internal standard. The above two solvents were chosen due to their ability to readily dissolve all the prepared ligands.

3.1.2.4.1 ^1H NMR studies

The ^1H NMR peak assignments of the prepared ligands is portrayed in the spectrum of ligand **L2** (figure 3-6). The peak assignments were performed according the chemical shift value of the relevant protons. The spectra of the remaining ligands **L1**, **L3**, **L4** and **L5** are located in the appendix section and table 3-4 gives a summary of all the peak values of all ligands.



Table 3-4: Proton NMR and elemental analysis data of ligands

Ligand	NMR (ppm)	Elemental analysis (Calc) %		
	HC=N	C	H	N
L1	7.82	65.72 (65.87)	5.70 (5.13)	16.1 (16.7)
L2	8.81	62.92 (62.10)	5.20 (4.82)	15.64 (15.49)
L3	8.31	56.64 (56.77)	3.66 (3.73)	15.24 (15.74)
L4	8.44	48.77 (48.78)	3.15 (2.93)	13.13 (13.22)
L5	8.83	54.55 (54.91)	19.57 (19.43)	3.57 (3.37)

Analysis of figure 3-6 above indicates that the condensation reaction of the Schiff base was successful since a strong peak of a single proton, characteristic of the imine functional group, is noticeable at 8.81 ppm and also the fact that there is no peak appearing in the region of 9.5 ppm to 10.5 ppm characteristic of the aldehyde functional group. This peak value for the azomethine functional group is in conformity with other related studies reported in literature [68, 72]. All the remaining ligands spectra in the appendix section display globally the same characteristics as figure 3-6 but with somewhat different values for the imine peak as listed in table 3-5. The imine peak values for the ligands range from 7.82 ppm to 8.83 ppm. This range is in conformity with the one published in literature for the azomethine functional group range [73].

Ligands **L1** and **L2**, which have activating substituents attached, are exhibiting imine peak values that are at opposite ends since **L1** has the lowest value of 7.82 ppm and **L2** has the second highest value of 8.81 ppm in table 3-4 above. **L3**, **L4** and **L5**, which have deactivating substituents attached, are displaying values that are 8.31 ppm, 8.44 ppm and 8.83 ppm respectively. It is noticeable that the imine peak values of **L3** and **L4** are less deshielded than that of **L2**, and only ligand **L5** has a higher chemical shift value. Theoretically **L3** and **L4** should have exhibited the highest imine peak values since they have chlorine (Cl) and bromine (Br) groups as their respective attached substituents.

3.1.2.4.2 ^{13}C NMR studies



UNIVERSITY of the
WESTERN CAPE

The following ^{13}C NMR spectrum of ligand **L2** (figure 3-7) is a typical spectrum of the prepared ligands in this study. The spectra for the remaining ligands **L1**, **L3**, **L4** and **L5** are displayed in the appendix section. Table 3-5 lists the chemical shift values of all ligands. The assignment of the carbon peak values of ligands was performed according to literature functional group chemical shifts values.

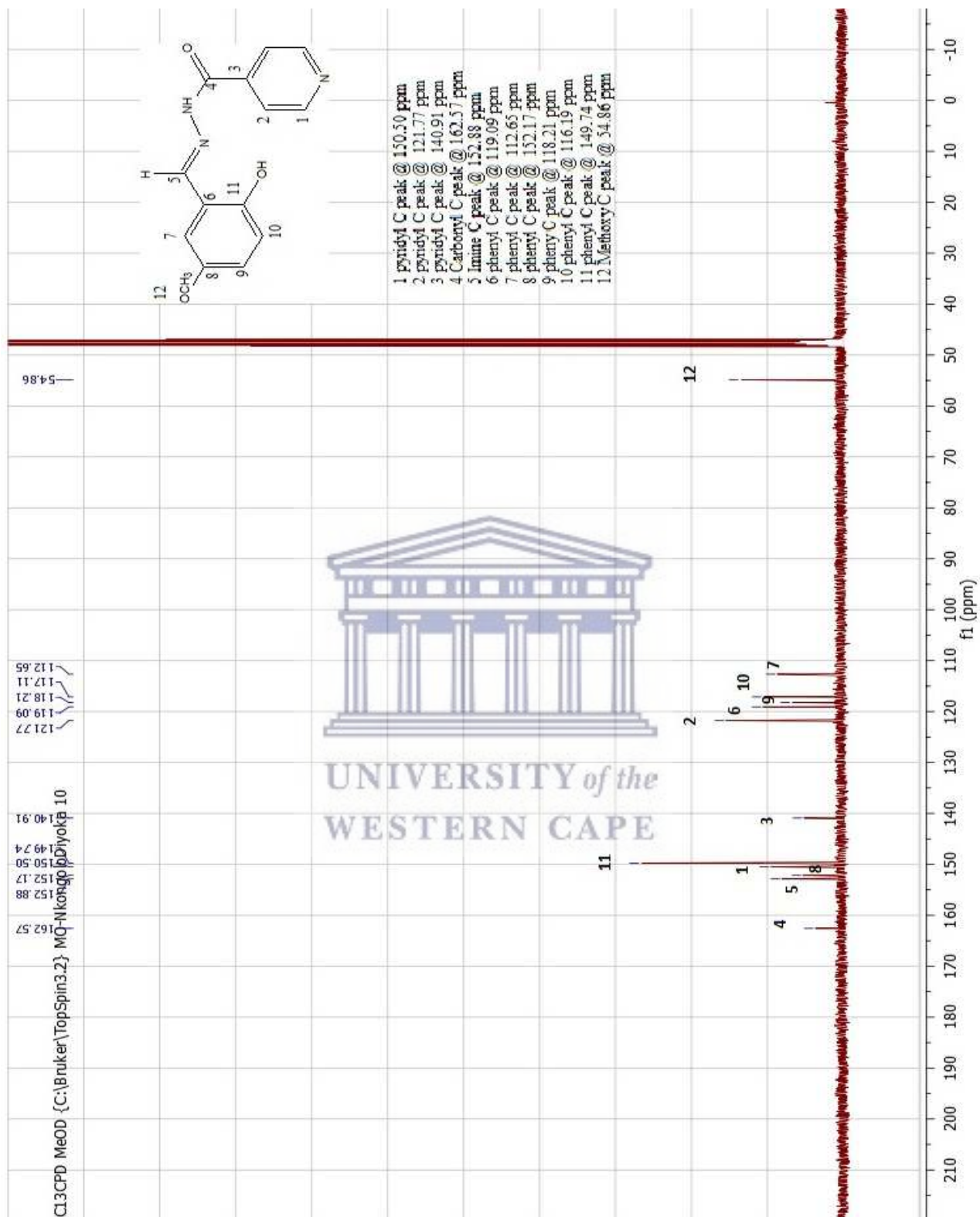


Figure 3-7: 13 C NMR of Isonicotinic acid (2-hydroxy-5-methoxy-benzilidene)-hydrazide (L2)

Table 3-5: ¹³C NMR data of ligands

Ligand	NMR Functional groups (PPM)	
	C=N	C=O
L1	151.55	162.37
L2	152.88	162.57
L3	155.96	161.97
L4	151.10	162.08
L5	151.7	163.22

Analysis of the above ¹³C NMR spectrum of ligand **L2** (figure 3-7) confirms the successful synthesis of the Schiff base since the imine carbon peak is appearing at 152.88 ppm chemical shift and no carbon peak, characteristic of the aldehyde functional group, is visible in the region of 195 to 205 ppm [73]. Given that figure 3-7 is an example of the spectra of all the ligands **L1** to **L5**, with minor differences due to their respective substituents, indicates the successful preparation of all ligands in this study. Furthermore all the ¹³C NMR peaks for each chemically different carbon are accounted for and assigned. Table 3.5 above displays the chemical shift values of the ¹³C NMR peak values for the azomethine and the amide carbonyl functional groups of all the ligands. Ferraresi-curroto V, Echeverrlla GA, Piro OE, et al. reported similar values in their work on hydrazones [51].

3.2 Ruthenium Complexes of Schiff base ligands

3.2.1 General remarks

Ruthenium is a unique metal found associated with other platinum metals such as pentlandite and pyroxinite because it has three oxidation states (+2, +3 and +4) that are biologically accessible [55]. Its discovery as a potential pharmacological agent is closely related to the use of cisplatin as a chemotherapeutic compound because it is less toxic while sharing similar ligand exchange properties [74]. Ruthenium (II) and (III) have the ability to afford six-coordinated octahedral geometries with the axial ligands fine-tuning the steric and electronic properties of the complexes [57]. Its three dimensional configuration, which makes possible the ligand coordination and functionalization aimed at specific molecular targets, renders it a suitable candidate for the design and synthesis of drug delivery systems [55].

The ruthenium (II) precursor used in this study was $\text{RuCl}_2(\text{DMSO})_4$. It was synthesized by dissolving two grams of $\text{RuCl}_3 \cdot x\text{H}_2\text{O}$ in 50 ml of ethanol according to literature procedure [17].

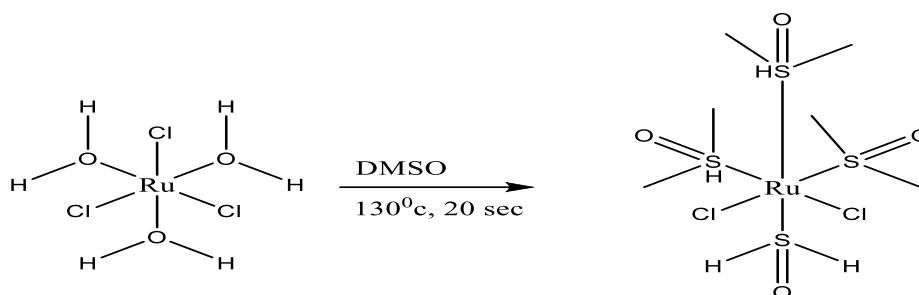


Figure 3-8: Scheme of the preparation of the ruthenium precursor, $\text{RuCl}_2(\text{DMSO})_4$

3.2.2 The complexes

All the synthesized complexes namely **C1**, **C2**, **C3**, **C4** and **C5** were prepared according to the same procedure (scheme 5) as referenced in literature [43, 75]. A one to one ratio of the ruthenium moiety and one of the five Schiff base ligand carrying different substituents on the metha position were taken together in an ethanolic solution under nitrogen atmosphere and reflux for four hours. All complexes were isolated as solid powder in good yield and stable at room temperature. They were all soluble in DMSO and partially soluble in water. Some complex products had the same color namely **C3** and **C4** that were pale brown. While the other products exhibited different colors. **C1** was light brown, **C2** was brittle-dark brown and **C5** was bright orange. All prepared complexes were subjected to FT – IR studies, UV – VIS studies, and NMR studies as well as elemental analysis.

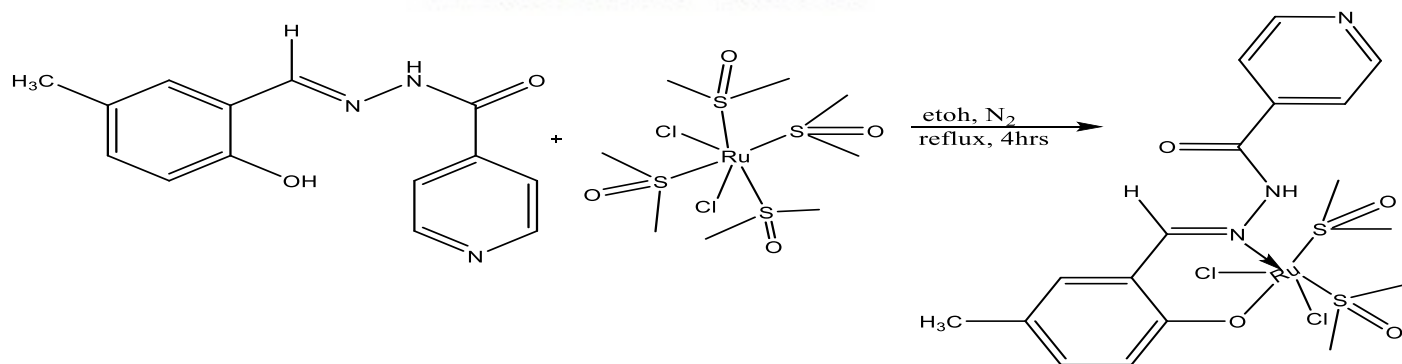


Figure 3-9 : Scheme of synthesis of $\text{C}_{18}\text{H}_{26}\text{Cl}_2\text{N}_3\text{O}_4\text{RuS}_2$, **C1**

3.2.2.1 Fourier transform infrared studies

The following spectrum of complex **C1** (figure 3-10) is a standard example of the spectrum obtained for all complexes prepared in this project. The spectra of the remaining complexes **C2**, **C3**, **C4** and **C5** are located in the appendix section. The main functional groups peak values are listed in table 3.6.

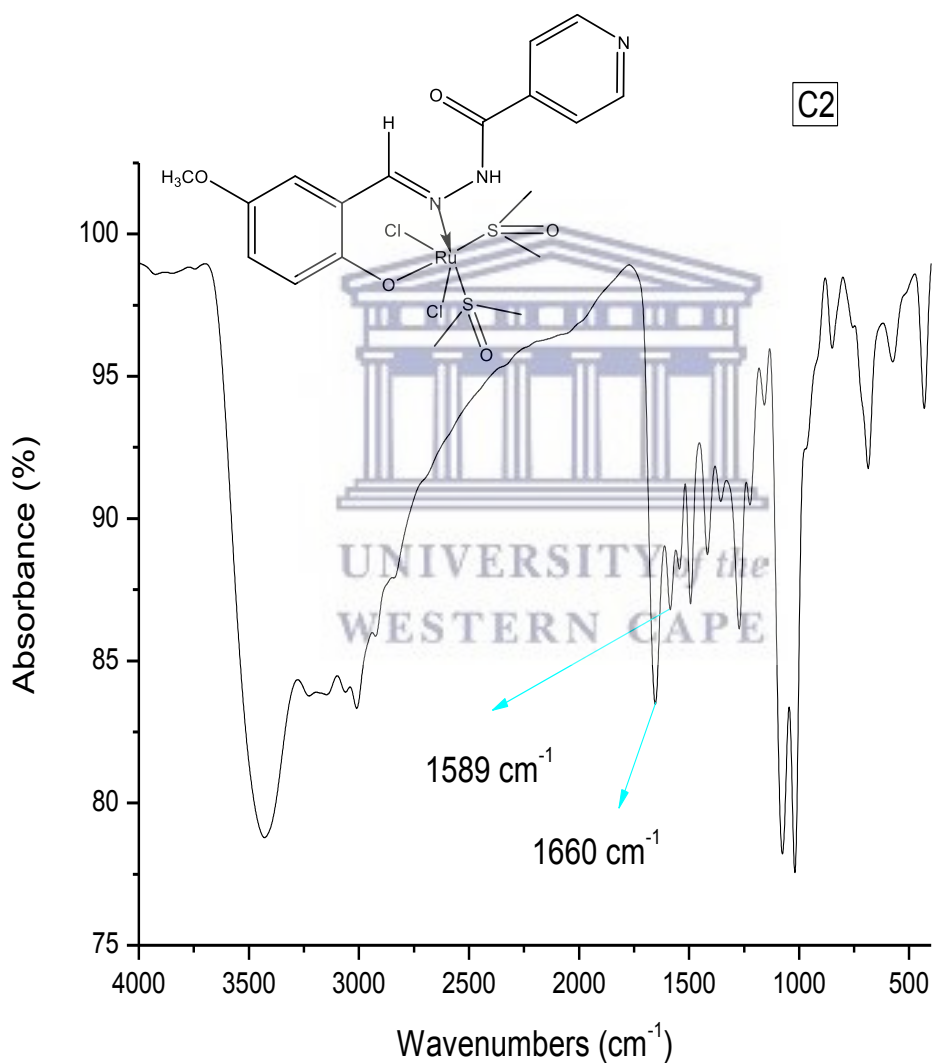


Figure 3-10: FTIR spectrum of complex **C2**

Table 3-6: FTIR data and percentage yield of complexes

Complex	FT – IR (cm ⁻¹)		% Yield
	C=O	C=N	
C1	1643	1536	69
C2	1640	1570	67
C3	1645	1540	65
C4	1650	1544	66
C5	1657	1543	73

Analyzing the Fourier transform infrared spectrum of complex **C2** (figure 3-10), it confirms the successful coordination of the Schiff base ligand to the metal precursor by exhibiting a shift of the azomethine or imine peak (C=N) from 1579 cm⁻¹ wave number in the free ligand to 1589 cm⁻¹ in the complex. This imine peak shift to 1589 cm⁻¹ coupled with the disappearance of the phenolic peak in the region of 3610 to 3670 cm⁻¹ indicate the successful coordination of the Schiff base ligand to the metal precursor. Raafat, M. et al and Bakirhan, M. et al reported similar imine peak shift values in their projects that are in agreement with other studies in literature [68, 72]. Also when comparing the imine peak values of the remaining complexes, namely **C1**, **C3**, **C4** and **C5**, in table 3-6 above to the azomethine peak values of their respective ligands, a shift in the peak values is noticeable for all of the complexes. The trend in the imine peak values shift is a blue shift for the majority of the complexes except for complexes **C2** and **C4**. Besides this shift in the imine peak values, no phenolic peak is displayed in the spectra of the complexes. These two facts further prove that the complexation occurred successfully.

Moreover there is a noticeable blue shift in the amide carbonyl peak values of all the complexes when compared to the values of this same functional group in their respective ligands per table 3-1.

3.2.2.2 Ultraviolet visible studies

UV – Vis absorption spectra of the complexes **C1** to **C5** were acquired using 1 cm micro cuvettes in ethanol solvent at room temperature in the wavelength range of 200 to 800 nm.

The following spectrum (figure 3-11) is a representative sample of the spectra obtained for the ruthenium complexes of Schiff base ligands prepared in this project **C1** to **C5**. A summary of all electronic transitions is displayed in table 3-7 and the remaining spectra of ligands **C2** to **C5** are located in the appendix section.

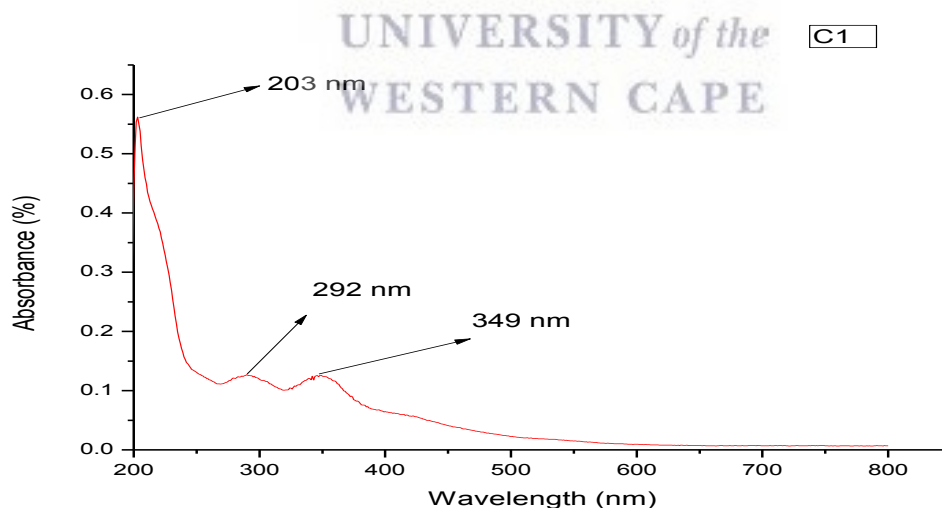


Figure 3-11: UV - VIS spectrum of complex C1

Table 3-7: UV - VIS data of complexes

Complex	Electronic transitions (nm)		
	$\pi \rightarrow \pi^*$	$n \rightarrow \pi^*$	λ_{max}
C1	203, 292	349	203
C2	205, 228, 255, 289	359	205
C3	203, 219, 288	345	203
C4	206, 218, 289	355	206
C5	203	345	203

UNIVERSITY of the
WESTERN CAPE

The prepared ruthenium complexes in this study are exhibiting electronic transitions in the range of 203 nm to 359 nm. All the complexes **C1** to **C5** display two to five absorption bands corresponding to two kinds of electronic transitions namely $\pi \rightarrow \pi^*$ and $n \rightarrow \pi^*$. When compared to their respective free ligands, all complexes **C1** to **C5** are displaying a shift in the transitions peak values for all absorption bands, whether they correspond to $\pi \rightarrow \pi^*$ and $n \rightarrow \pi^*$ transitions. The shift in the lower wavelength region assigned to $n \rightarrow \pi^*$ transitions of the azomethine (C=N) functional group ranges from 2 nm to 21 nm. This shift in $n \rightarrow \pi^*$ transitions for all complexes is evidence of the coordination of the imine nitrogen of all ligands to the

metal precursor, and therefore of the successful synthesis of the complexes [76]. Sharmal et al. reported similar findings in their study about comparative preparation methods of Schiff base ligands and their complexes [77]. Also the fact that a shift is noticeable in the absorption peak values of the higher region, corresponding to the $\pi \rightarrow \pi^*$ transitions for all complexes versus their respective free ligands, is proof that coordination is also occurring between the metal precursor and the phenolic oxygen [78].

3.2.2.2.1 TGA of complexes

Figure 3-12 of complex **C5** below is a good example of the TGA graphs of all complexes **C3** to **C5**. Table 3-8 exhibits all the decomposition stages of all complexes as well as the assignments of the relative mass losses.



C5

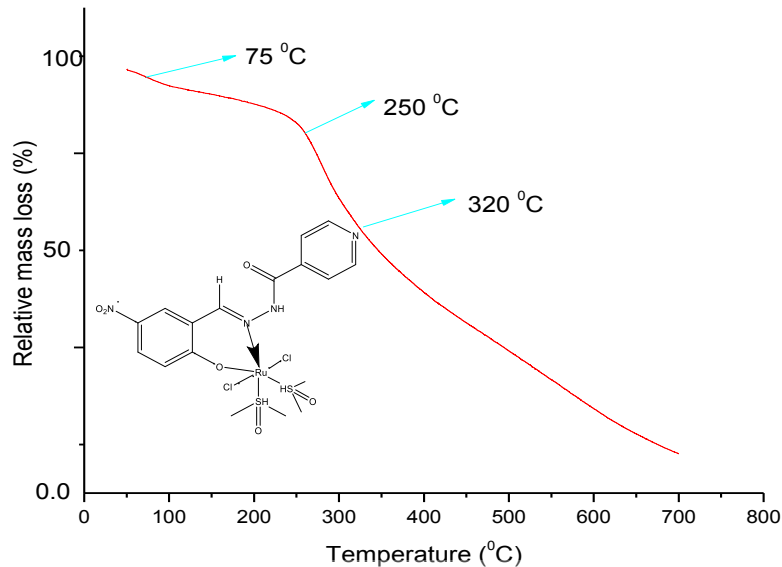


Figure 3-12: TGA graph of complex C5

Table 3-8: TGA data of complexes

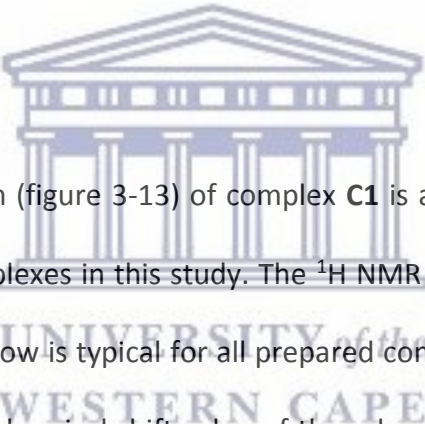
Complex	Temperature range (°C)	Mass loss %	Assignments
		Calc/Found	
C3	75 °C – 250 °C	2.3 (3.2)	(H ₂ O)
	250 °C – 370 °C	9.5 (11.1)	(Cl ₂)
	370 °C – 700 °C	59.4 (60.8)	(C ₄ H ₁₄ Cl ₂ O ₃ RuS ₂)
C4	75 °C – 250 °C	5.7 (6.5)	(H ₂ O)
	250 °C – 370 °C	12.86 (11.75)	(Cl ₂)
	370 °C – 700 °C	66.1 (67.03)	(C ₄ H ₁₄ Cl ₂ O ₃ RuS ₂)
C5	75 °C – 250 °C	4.1 (3.4)	(H ₂ O)
	250 °C – 320 °C	33.3 (34.8)	(C ₁₃ H ₉ N ₃ O)
	320 °C – 700 °C	61.3 (63.1)	(C ₄ H ₁₄ Cl ₂ O ₃ RuS ₂)

According to figure 3-12 of complex **C3** and table 3-8, all tested complexes **C3** to **C5** are exhibiting three stages of decomposition and all are stable from 50 °C to 75 °C. The above fact is different to their respective ligands as far as number of decomposition stages and temperature stability. Per table 3-8, it is highly noticeable that the first decomposition stage of all three complexes is corresponding to the relative mass of water molecule (H₂O). Two complexes **C1** and **C2** are exhibiting exactly the relative mass loss of the same compounds for all of their stages at slightly different percentage. Only complex **C3** displaying a different molecule mass loss at its second decomposition stage. The stage one for all complexes **C3**, **C4** and **C5** is starting from 75 °C – 250 °C corresponding to the relative mass loss of water at 2.3 % (calc. 3.2 %), 5.7 % (calc 6.5 %) and 4.1 % (calc. 3.4 %) respectively. The stage two for all complexes is starting from 250 °C – 370 °C and corresponds to the relative mass loss of the chlorine molecule (Cl₂) for complexes **C3** and **C4** at 9.5 % (calc. 11.1 %) and 12.86 % (calc. 11.75 %) respectively, but for **C5** it corresponds to a mass loss of 33.33 % (calc. 34.8 %) for the moiety (C₁₃H₉N₃O). The third and last stage of decomposition for all complexes corresponds to the mass loss of the moiety (C₄H₁₄Cl₂O₃RuS₂) at different percentages 59 % (calc. 60.8 %) for **C1**, at 66 % (calc. 67.03 %) for **C4** and at 61.3 % (calc. 63.1 %) for **C5**. Some scientists have reported similar findings about thermal work on complexes of Schiff base ligands [71, 79].

3.2.2.3 Nuclear magnetic resonance studies

In order to confirm the coordination of all five synthesized complexes **C1 – C5**, proton (^1H) NMR was performed for this purpose. The deuterated solvent deemed suitable to perform the NMR characterization is deuterated dimethyl sulfoxide at room temperature using trimethyl silane (TMS) as internal standard. The above solvent was selected because it was able to readily dissolve all the prepared complexes.

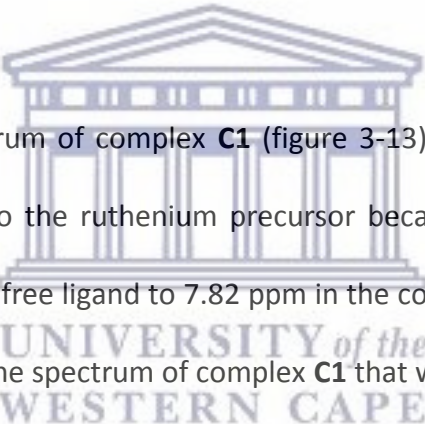
3.2.2.3.1 ^1H NMR studies



The following ^1H NMR spectrum (figure 3-13) of complex **C1** is a characteristic example of the spectra of the synthesized complexes in this study. The ^1H NMR peak assignments displayed in the spectrum of complex **C1** below is typical for all prepared complexes. The peak assignments were performed according the chemical shift value of the relevant protons. The spectra of the remaining complexes **C1**, **C3**, **C4** and **C5** are located in the appendix section and table 3-9 gives a summary of all the peak values for all complexes.

Table 3-9: Proton NMR and elemental analysis data of complexes

Complex	NMR (ppm)	Elemental analysis(Found) %		
	HC=N	C	H	N
C1	8.00	32.20(31.47)	4.15(4.52)	7.21(7.19)
C2	7.94	32.12(31.24)	4.04(4.12)	7.02(6.91)
C3	8.66	33.87(33.57)	3.51(3.60)	6.97(6.61)
C4	7.98	31.54(30.98)	3.27(3.47)	6.61(6.41)
C5	7.82	33.28(32.97)	3.45(3.75)	9.13(9.65)



Careful inspection of the spectrum of complex **C1** (figure 3-13) above exhibits the successful coordination of the ligand **L1** to the ruthenium precursor because the imine peak value has shifted from 8.00 ppm from the free ligand to 7.82 ppm in the complex. Also the disappearance of the phenolic proton peak in the spectrum of complex **C1** that was showing in the spectrum of its respective ligand **L1** at 9.02 ppm is indicative of the coordination of the ruthenium precursor to the ligand **L1** via its phenolic oxygen. Jian-ning, L et al. reported similar findings in his project about the synthesis and characterization of metal complexes with tetradentate Schiff bases [78]. Analysis of the imine peak values of the remaining complexes namely **C2**, **C3**, **C4** and **C5** in table 3-9 above exhibits a shift from the imine peak values of their respective free ligands **L2**, **L3**, **L4** and **L5**. The shift margin ranges from 0.18 ppm to 1.01 ppm. This fact combined with the disappearance of the phenolic proton peak in all the remaining complexes consecrate the successful preparation of all complexes.

Chapter 4: Antimicrobial studies

4.1 General remarks

Microbes are the tiny microorganisms that inhabit the world with us, around us and even in us. They are living things that possess one cell or multiple cells and are classified as bacteria, protozoa, fungi and algae. Some of them are beneficial to the human body and others are cause of diseases in the human body [80]. In light of this, the scientific community has to continually strive to develop new chemicals or compounds to neutralize pathogenic microbe which are a threat to our health.

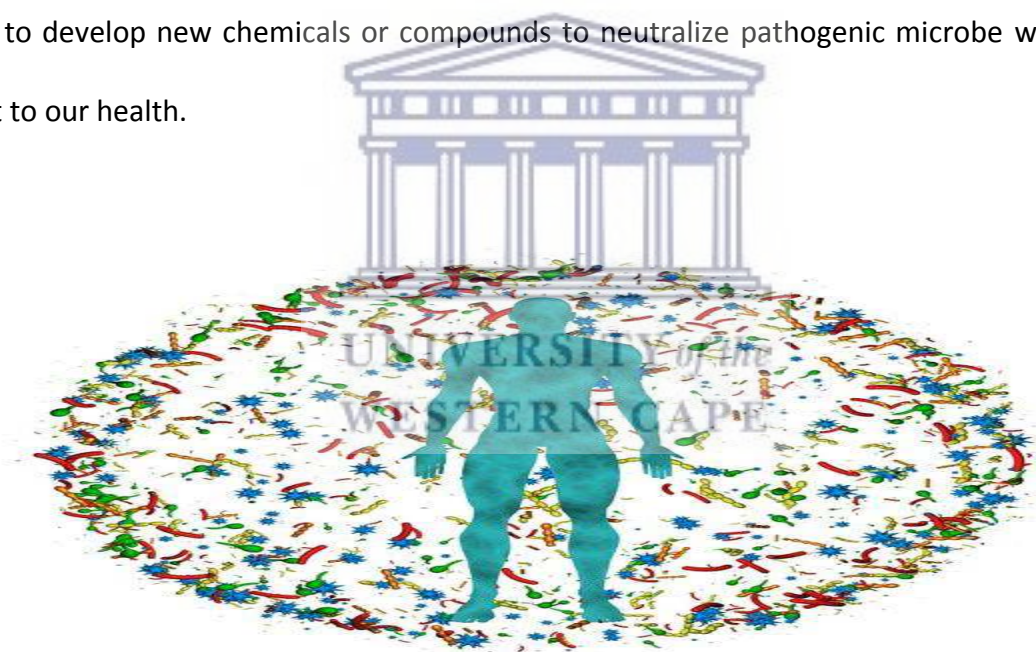


Figure 4-1: Image of microbes surrounding a human body

Hence, the synthesized free ligands and their respective ruthenium complexes were standardly tested against two kinds of microorganisms, namely Gram negative and Gram positive.

Two Gram positive microorganisms were used; *Staphylococcus aureus* (*S. Aureus*, ATCC no. 25923) and Methicillin resistant *Staphylococcus aureus* (MRSA, ATCC no. 33591), and one Gram negative microorganism, namely *Pseudomonas aeruginosa* (*P aeruginosa*, ATCC 27853).

4.2 Screening of the antibacterial activity

4.2.1 Preparation of test samples

All compounds were dissolved in DMSO since all were indicated to be soluble in the solvent. Two concentrations were prepared for the experiment: 1mg of test compound dissolved in 1 mL of solvent and then further diluted with a 1:10 dilution ratio.

The formula for calculating the test compound concentrations was as follows:

$$\text{Concentration} = [\text{mass/molecular weight}]/\text{volume}$$

UNIVERSITY of the
WESTERN CAPE

4.2.2 Agar disk diffusion assay

Agar diffusion techniques are preliminary screening methods that have been widely used to assay plant extracts for antimicrobial activity [83]. Sterile 9 mm disks were impregnated with 50 μ l of dissolved compounds (at two concentrations) and incubated at 37 $^{\circ}$ c for 24 hours to dry. The positive control substances used was the broad spectrum antibiotic ampicillin and DMSO was used as the negative control. A suitable solid agar medium was inoculated with the respective test organisms (inoculum size: 1×10^8 CFU/ml of bacteria) [84]. The media utilized

in this assay was Mueller Hinton agar, described as the medium of choice by Ncube and colleagues [85]. The dried paper disks, saturated with the test compounds at desired concentrations, together with the positive and negative controls were then placed carefully onto the surface of the pre-inoculated agar. The plates were then incubated at 37 °C for 24 hours. The inhibition zones were measured in millimeters (mm) from the circumference of the disk to that of the growth-free zones around the disk and recorded. All samples were tested in duplicates.

4.3 Results of antimicrobial activity

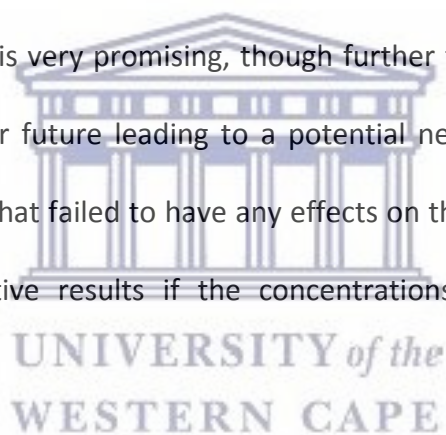
Antibacterial activities of the compounds were evaluated against Gram positive and Gram negative bacteria using agar well diffusion. The bacteria were exposed to 10 µL of 100 µg/mL stock solution (equivalent to 1 µg concentration of the compounds) for 24 hours, the bacterial activity was assessed based on the diameter of the clearing zone (zone of inhibition). As shown in Figure 4-2, nine of the ten compounds did not show any activity against the three tested bacterial strains. *S aureus* was the only strain that showed susceptibility to **L5**, as indicated by the zone of inhibition observed around the compound. The same compound did not show any activity on the other two strains.

The susceptibility of *Staphylococcus aureus* to ligand **L5** makes this antimicrobial result very interesting because *S. aureus* is one of the microorganisms that are mostly responsible for some common and deadly infections in humans. An example of one of these deadly infections

is *Staphylococcus aureus bacteremia* (SAB) which leads to one of its deadly conditions called infective endocarditis (IE) [86].

SAB has become a serious medical problem because of its occurrence and the poor results obtained in patients treatments. SAB is ranked at the top of the list of blood stream infections in the developed world. For instance in the United States, a 283 percent increase in the occurrence of nosocomial SAB infections was observed during the period of 1980 to 1989 [86].

In light of the seriousness of the infections caused by this commensal bacterium to humans, new drugs for treatment and prevention strategies are of the essence. Hence, ligand **L5** results at 1 microgram concentration is very promising, though further tests at higher concentrations shall be conducted in the near future leading to a potential new drug. Also, the rest of the ligands and all the complexes that failed to have any effects on the three bacteria tested might be able to show some positive results if the concentrations are somewhat significantly increased.



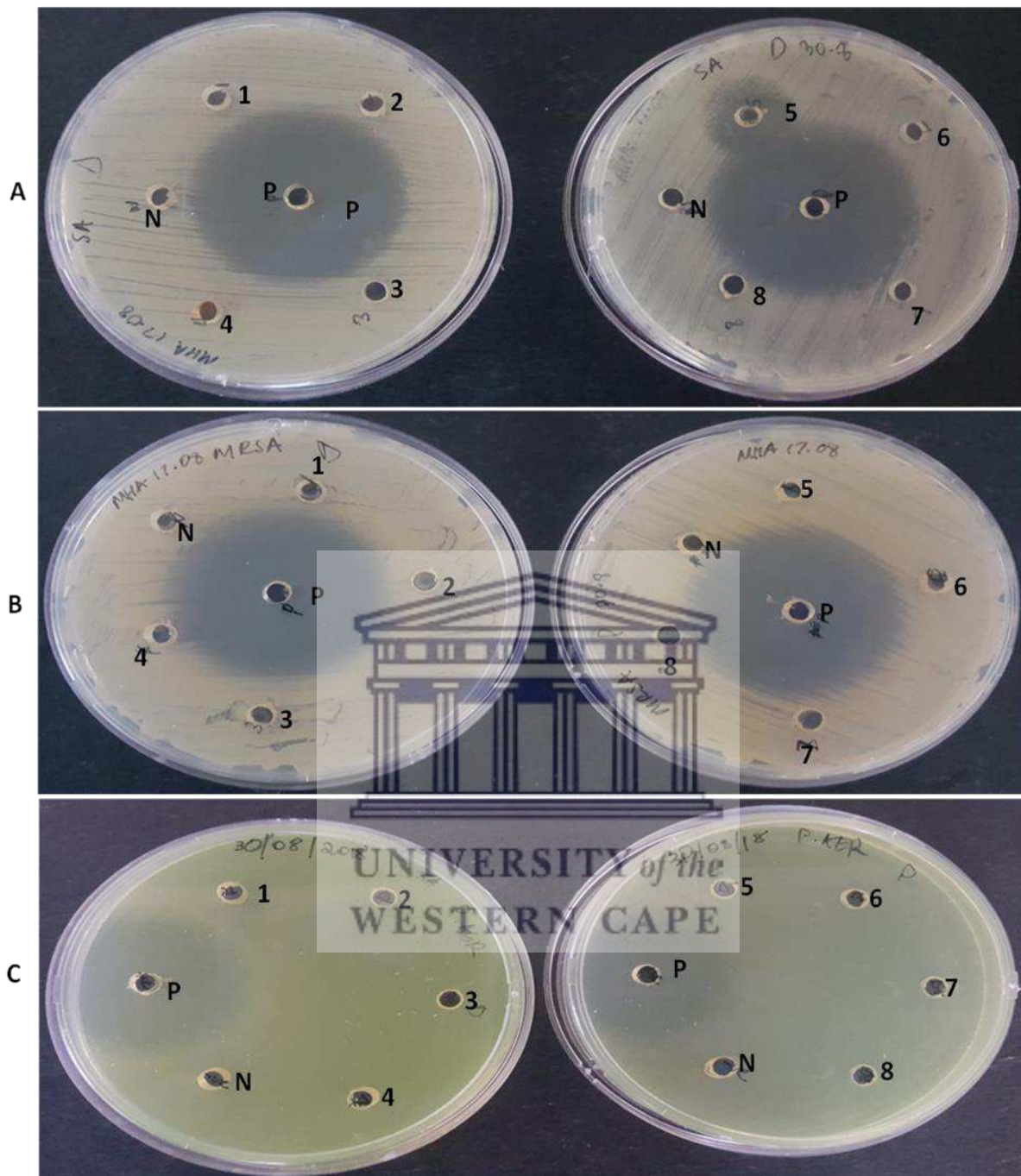


Figure 4-2: The antibacterial activity against *S. aureus* (A), MRSA (B) and *P. aeruginosa*. P= Positive control (Ampicillin), N= negative control (diluent), 1= L3, 2= L4, 3= C3, 4= C4, 5= L5, 6=C5, 7= C2, 8 = C1.

Chapter 5: Conclusion and recommendations

5.1 Conclusion

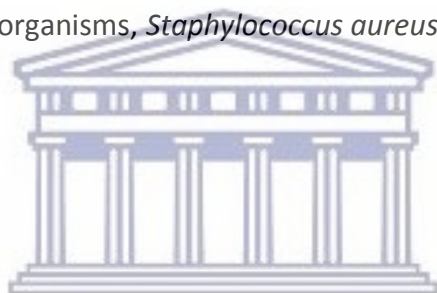
This project entailed the synthesis of (arene) ruthenium (II) complexes of isoniazid Schiff base ligands that exhibit good antimicrobial properties. All the Isoniazid Schiff base ligands were successfully prepared and obtained as solids in good yields 59 to 72 percent. Ligands **L1** to **L5** were found to be stable at room temperature and soluble in most polar organic solvents. They were all fully characterized by FTIR, UV – VIS, TGA, NMR and elemental analysis.

FTIR confirmed the successful preparation of **L1** – **L5** by the exhibition of the imine functional group band in the range of 1541 cm^{-1} to 1579 cm^{-1} , UV – VIS also confirmed it by displaying $n - \pi^*$ electronic transitions corresponding to the azomethine functional group in the range of 324 nm to 355 nm, NMR spectroscopy confirmed it as well by the appearance of ^1H NMR peaks in the range of 7.82 ppm to 8.83 ppm and ^{13}C NMR peaks in the range of 151.10 ppm to 155.96 ppm. Elemental analysis results further confirmed the success of the Schiff base ligands preparation. TGA studies attested the thermal stability of ligands **L3** to **L5**.

Ligands **L1** to **L5** all underwent equimolar complexation reaction with the ruthenium precursor $\text{RuCl}_2(\text{DMSO})_4$ to yield ruthenium (II) Schiff base ligand complexes **C1** to **C5**. All the complexes were obtained as solids in good yields of 69 to 73 percent. They were found to be stable at room temperature but only soluble in dimethyl sulfoxide. The confirmation of the successful

complex preparation was verified by conducting FTIR, UV – VIS and NMR studies that all display shifts in the values of the imine functional group bands, electronic transitions as well as peaks when compared to the imine values of the respective ligands of each synthesized complex. TGA studies ascertained the stability of the complexes for antimicrobial applications.

All the compounds ligands **L1** to **L5** as well as their respective complexes **C1** to **C5** were tested for antimicrobial activities against two Gram negative microorganisms *Staphylococcus aureus* and Methicillin resistant *Staphylococcus aureus*, and one Gram positive bacteria *Pseudomonas aeruginosa*. Only ligand **L5** out of the ten prepared compounds showed antibacterial activity against only one of three microorganisms, *Staphylococcus aureus*.



UNIVERSITY of the
WESTERN CAPE

5.2 Recommendations

All the isoniazid Schiff base ligands and their respective complexes were successfully prepared and characterized by various spectroscopic and analytical techniques as well as tested for their biological activities against three microorganisms. Nevertheless, some recommendations that can be made are listed below;

- Crystallography should be done for all ligands and complexes
- Biological activity studies against resistant strains of *M. tuberculosis* bacteria should be undertaken for all ligands and complexes

References

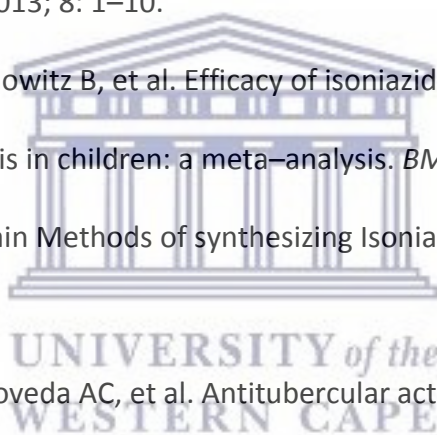
- [1] Heryanto R, Hasan M, Abdullah EC. Short Article Solubility of Isoniazid in Various Organic Solvents from (301 to 313) K Solubility of Isoniazid in Various Organic Solvents from (301 to 313) K. *Engineering* 2008; 53: 1962–1964.
- [2] WHO. *Global Tuberculosis Report 2017: Leave no one behind - Unite to end TB*. Epub ahead of print 2017. DOI: 10.1001/jama.2014.11450.
- [3] Daniel TM. The history of tuberculosis. *Respir Med* 2006; 100: 1862–1870.
- [4] Hayman J. Mycobacterium Ulcerans: an Infection From Jurassic Time? *Lancet* 1984; 2: 1015–1016.
- [5] Kapur V, Whittam TS, Musser JM. Is mycobacterium tuberculosis 15,000 years old? *J. Infect Dis* 1994;170: 1348-9.
- [6] The evidence for the incidence of tuberculosis in ancient Egypt. *Br J Tuberc* 1939; 33: 142-52.
- [7] Hirsh Ae, Tsolaki Ag, Dereimer K, Feldman Mw, Small Pm. Stable association between strains of Mycobacterium tuberculosis and their human populations. *Proc Natl Acad sci USA* 2004; 101: 4871-6.
- [8] Gutierrez Mc, Brisse S, Brosch R, Fabre M, Omais B, Marmiesse M, et al. Ancient origin and gene mosaicism of the progenitor of Mycobacterium tuberculosis. *Pcos Pathog* 2005; 1: e5.

- [9] Morse D. Tuberculosis. In: Brothwell D, Sandison At, editors. Diseases in antiquity. A survey of the disease, Injuries and survey of early populations. Springfield, Il: Charles C. Thomas; 1967.
- [10] Caon T, Campos CEM, Simões CMO, et al. Novel perspectives in the tuberculosis treatment: Administration of isoniazid through the skin. *Int J Pharm* 2015; 494: 463–470.
- [11] Tripathi RP, Tewari N, Dwivedi N, et al. Fighting tuberculosis: An old disease with new challenges. *Med Res Rev* 2005; 25: 93–131.
- [12] Pavan FR, Poelhsitz G Von, do Nascimento FB, et al. Ruthenium (II) phosphine/picolinate complexes as antimycobacterial agents. *Eur J Med Chem* 2010; 45: 598–601.
- [13] Jnawali HN, Ryoo S. First – and Second – Line Drugs and Drug Resistance. *Tuberc issues diagnosis Manag* 2013; 163–180.
- [14] Hazbon MH, Brimacombe M, Bobadilla del Valle M, et al. Population genetics study of Isoniazid resistance mutations and evolution of Multidrug resistant Mycobacterium tuberculosis. *Antimicrob Agents Chemother*. 2006; 50: 2640-2649.
- [15] Argyson A, Jin L, Siconilfibaez L, Angeletti RH, Blanchard JS. Proteomewide profiling of Isoniazid targets in Mycobacterium tuberculosis. *Biochemistry*. 2006; 45: 13947-13953.
- [16] Timothy MD. Tuberculosis: Diagnosis and treatment. Wallingford, Oxfordshire: CABI; 2011: 219.
- [17] When I use a word. I mean it. *Br J Med*. 1991; 319 (october): 972.
- [18] Schatz A, Waksman SA. Effect of Streptomycin and other antibiotic substances upon Mycobacterium tuberculosis and related organisms. *Exp Biol Med*. 1944; 57: 244-248.
- [19] Fox W, Ellard GA, Mitchson DA. Studies on the treatment of tuberculosis undertaken by

- the British Medical Research Council tuberculosis units, 1946-1986, with relevant subsequent publications. *Int J. tuberc Lung Dis.* 1999; 3: 5231-5279.
- [20] Yeager RL, Munroe WG, Dessau FI. Pyrazinamide (aldinamide) in the treatment of pulmonary tuberculosis. *Am Rev Respir Dis* 1952; 65: 523-546.
- [21] Ando H, Miyoshiakiyama T, Watanabe S, Kirikae T. A silent mutation in *mabA* confers isoniazid resistance in *Mycobacterium*. *Mol Microbiol.* 2014; 91: 538-547.
- [22] Thomas JP, Baughn CO, Wilkinson RG, Shepherd RG. A new synthetic compound with antituberculous activity in mice: ethambutol (destro-2,2'-(ethylenediamino)-di-1-butanol). *Am Rev Respir Dis.* 1961; 83: 891 - 893.
- [23] Karlson AG. The in vitro activity of ethambutol (dextro-2,2'-[ethylenediimino]-di-1-butanol) against tubercle bacilli and other microorganisms 1. *Am Rev Respir Dis.* 1961; 84: 905 - 906.
- [24] Wilkinson RG, Cantrall MB, Shepherd RG. Antituberculous agents. III(+)-2,2-(ethylenediimino)-di-1-butanol, 1,1 and some analogs. *J Med Chem.* 1962; 5: 835 - 845.
- [25] Edson RS, Terrell CL. The Amiglycosides. *Mayo clin Proc.* 1991; 66: 1158 - 1164.
- [26] Comroe Jr JH. Pay dirt: the story of Streptomycin: Part II. Feldman and Hinshaw; Lehmann. *Am Rev Respir Dis.* 1978;117: 957 - 968.
- [27] Kingston W. Streptomycin, Schatz V. Waksman, and the balance of credit for discovery. *J Hist Med Allied Sci.* 2004; 59: 441 - 462.
- [28] Fabregas A, Madurga S, Giralt E, Vila J. Mechanism of action of and resistance to quinolones. *Microb Biotechnol.* 2009;2:40-61.
- [29] Goss WA, Deytz WH, Cook TM. Mechanism of action of nalidixic acid on *Escherichia coli*

- II. Inhibition of deoxyribonucleic acid synthesis. *J Bacteriol.* 1965;89:1068-1074.
- [30] Vilcheze C, Wang F, Arai M, et al. Transfer of point mutation in *Mycobacterium tuberculosis inhA* resolves the target of Isoniazid. *Nat Med.* 2006;12:1027-1029.
- [31] Vasava MS, Bhoi MN, Rathwa SK, et al. Drug development against tuberculosis: Past, present and future. *Indian J Tuberc* 2017; 64: 252–275.
- [32] Garland J. Kanamycin (editorial). *N Engl J Med.* 1958;5:397-406.
- [33] Farmer P, Kim JY. Community based approaches to the control of multidrug resistant tuberculosis: Introducing 'DOTS-plu'. *Br Med J.* 1998;317:671.
- [34] Sutton WB, Gordee RS, Wick WE, Stanfield L. In vitro and in vivo laboratory studies on the antituberculous activity of capreomycin. *Ann NY Acad sci.* 1966;135:947-959.
- [35] Umezawa H. Kanamycin: its discovery. *Ann NY Acad Sci.* 1958;76:20-26.
- [36] Powers T, Noller HF. Selective perturbation of G530 of 16s rRNA by translational miscoding agents and a streptomycin-dependence mutation in protein S12. *J Mol Biol.* 1994;235:156-172.
- [37] Bilgin N, Claesens F, Pahverk H, Ehrenberg M. Kinetic properties of *Escherichia coli* ribosomes with altered forms of S12. *J Mol Biol.* 1992;224:1011-1027.
- [38] Karimi R, Ehrenberg M. Dissociation rates of peptidyl-trna from the P-site of *E. coli* ribosomes. *Embo J.* 1996;15:1149-1154.
- [39] Sun Z, Zhang J, Zhang X, Wang S, Zhang Y, Li C. Comparison of *gyrA* gene mutations between laboratory selected ofloxacin resistant *Mycobacterium tuberculosis* strains and clinical isolates. *Int J Antimicrob Agents.* 2008;31:115-121.
- [40] Rengarajan J, Sasseti CM, Naroditskaya V, Sloutsky A, Bloom BR, Rubin EJ. The folate

- pathway is a target for resistance to the drug para-aminosalicylic acid (PAS) in mycobacteria. *Mol Microbiol.* 2004;53:275-282.
- [41] Sousa EHS, Basso LA, Santos DS, et al. Isoniazid metal complex reactivity and insights for a novel anti-tuberculosis drug design. *J Biol Inorg Chem* 2012; 17: 275–283.
- [42] Buczkowska MK. Synthesis, characterisation, antitumor and antimicrobial activities of heterocyclic transition metal complexes. 2011; 1–199.
- [43] Pavan FR, Poelhsitz G V., da Cunha LVP, et al. In Vitro and In Vivo Activities of Ruthenium(II) Phosphine/Diimine/Picolinate Complexes (SCAR) against Mycobacterium tuberculosis. *PLoS One* 2013; 8: 1–10.
- [44] Ayieko J, Abuogi L, Simchowitz B, et al. Efficacy of isoniazid prophylactic therapy in prevention of tuberculosis in children: a meta-analysis. *BMC Infect Dis* 2014; 14: 91.
- [45] Vrabete SS, Modra D. Main Methods of synthesizing Isoniazid in laboratory. *Ser Chem* 2013; 22: 77–84.
- [46] De Aguiar I, Tavares A, Roveda AC, et al. Antitubercular activity of Ru (II) isoniazid complexes. *Eur J Pharm Sci* 2015; 70: 45–54.
- [47] Tajudeen SS, Kannappan G. Indian Journal of Advances in Chemical Science Schiff Base – Copper (II) Complexes : Synthesis , Spectral Studies and Anti-tubercular and Antimicrobial Activity. 2016; 40–48.
- [48] Rickman KA, Swancutt KL, Mezyk SP, et al. Isoniazid: Radical-induced oxidation and reduction chemistry. *Bioorganic Med Chem Lett* 2013; 23: 3096–3100.
- [49] Chakraborty S, Rhee KY. Tuberculosis Drug Development: History and Evolution of the Mechanism-Based Paradigm. *Cold Spring Harb Perspect Med* 2015; 5: 11.



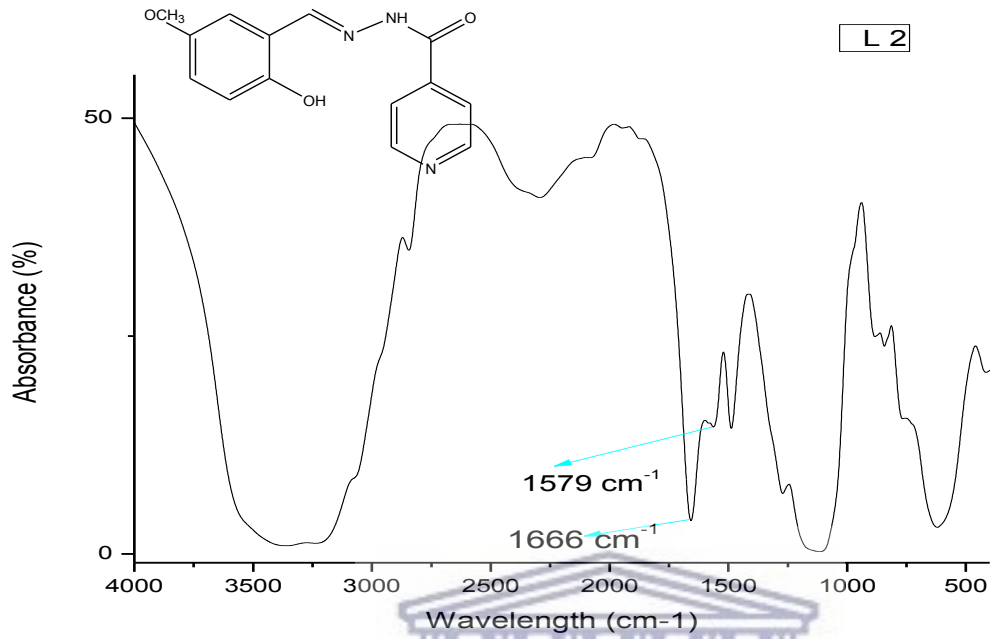
- [50] Ayieko J, Abuogi L, Simchowitz B, et al. Efficacy of isoniazid prophylactic therapy in prevention of tuberculosis in children: a meta-analysis. *BMC Infect Dis* 2014; 14: 91.
- [51] Ferraresi-Curotto V, Echeverría GA, Piro OE, et al. Synthesis and characterization of a series of isoniazid hydrazones. Spectroscopic and theoretical study. *J Mol Struct* 2017; 1133: 436–447.
- [52] Schiff H, Schiff T. Chapter – iii Synthesis , Characterization and Photo-Luminescent Properties of Schiff Base Metal Complexes.
- [53] Al-Garawi ZSM, Tomi IHR, Al-Daraji AHR. Synthesis and characterization of new amino acid-schiff bases and studies their effects on the activity of ACP, PAP and NPA enzymes (In Vitro). *E-Journal Chem* 2012; 9: 962–969.
- [54] Xavier A, Srividhya N. Synthesis and Study of Schiff base Ligands. *IOSR J Appl Chem* 2014; 7: 6–15.
- [55] Southam HM, Butler JA, Chapman JA, et al. *The Microbiology of Ruthenium Complexes*. 1st ed. Elsevier Ltd. Epub ahead of print 2017. DOI: 10.1016/bs.ampbs.2017.03.001.
- [56] Pal S, Pal S. Ruthenium(III) Complexes with a Phenolate-O, Imine-N, and Amide-O Coordinating Ligand: Syntheses, Structures, Properties, and Protonation Studies of Coordinated Amide. *Eur J Inorg Chem*. Epub ahead of print 2003. DOI: 10.1002/ejic.200300232.
- [57] Dragutan I, Dragutan V, Demonceau A. *Editorial of special issue ruthenium complex: The expanding chemistry of the ruthenium complexes*. 2015. Epub ahead of print 2015. DOI: 10.3390/molecules200917244.
- [58] Dharmaraj N, Viswanatharmurthi P, Natarajan K. Ruthenium (II) complexes containing

- bidentate Schiff² bases and their antifungal activity. *Transit Met Chem* 2001; 26: 105–109.
- [59] Colthup NB, Daly LH WS. *Introduction to Infrared and Raman Spectroscopy (Third Edition)*. Third edit. Elsevier, 1990.
- [60] King PL, Ramsey MS, McMillan PF, et al. Laboratory fourier transform infrared spectroscopy methods for geologic samples. *Infrared Spectrosc Geochemistry, Explor Geochemistry Remote Sens* 2004; 57–91.
- [61] Clark T, Frost T RM. Techniques, instrumentation and data handling. *Springer Sci Bus media*; 4,1993.
- [62] Morrell D. *Catalysis of Organic Reactions, CRC. Press., Science, 2002, 593. 2002.*
- [63] Thermo Spectronic. Basic UV-Vis Theory , Concepts and Applications Basic. *ThermoSpectronic* 2013; 1–28.
- [64] T. O. Fundamentals of modern UV-visible spectroscopy. *Hewlett-Packard Co* 1996; 38–61.
- [65] Finkelstein DM, Schumacker RE, Lomax RG. A Beginner's Guide to Structural Equation Modeling. *Technometrics* 2005; 47: 522–522.
- [66] [Http://www.slideshare.net/Kalsoommohammed/thermogravimetry-analysis-tga](http://www.slideshare.net/Kalsoommohammed/thermogravimetry-analysis-tga);
accessed on 11 October 2018.
- [67] [Http://sustainability.sellafieldsites.com/ressources/labmouse/chemistry_a2/2908.php](http://sustainability.sellafieldsites.com/ressources/labmouse/chemistry_a2/2908.php);
accessed on 10 October 2018.
- [68] Issa RM, Khedr AM, Rizk H. ¹H NMR , IR and UV / VIS Spectroscopic Studies of Some Schiff Bases Derived From 2-Aminobenzothiazole and 2-Amino-3-hydroxypyridine. *J Chinese Chem Soc* 2008; 55: 875–884.

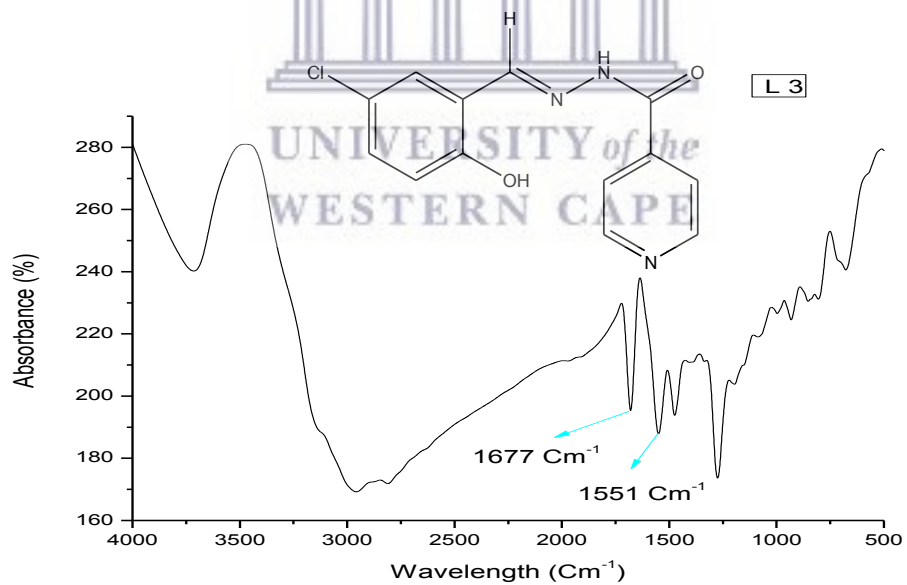
- [69] Singh HL, Singh J. Synthesis, spectroscopic, molecular structure, and antibacterial studies of dibutyltin(IV) Schiff base complexes derived from phenylalanine, isoleucine, and glycine. *Bioinorg Chem Appl*; 2014. Epub ahead of print 2014. DOI: 10.1155/2014/716578.
- [70] Hussain Z, Yousif E, Ahmed A, et al. Synthesis and characterization of Schiff's bases of sulfamethoxazole. *Org Med Chem Lett* 2014; 4: 1.
- [71] Guo J, Zhang J, Shu P, et al. Two new diterpenoids from the buds of *Wikstroemia chamaedaphne*. *Molecules* 2012; 17: 6424–6433.
- [72] Al-Rashdi KS, Eltayeb NE, Al-Khathami ND, et al. Synthesis of novel pyridyl-based schiff base and its coordination behaviour with ruthenium(II) and zinc(II). *Asian J Chem* 2017; 29: 1839–1844.
- [73] *Structure Determination of Organic Compounds*. Epub ahead of print 2009. DOI: 10.1007/978-3-540-93810-1.
- [74] Gambino D, Otero L. Perspectives on what ruthenium-based compounds could offer in the development of potential antiparasitic drugs. *Inorganica Chim Acta* 2012; 393: 103–114.
- [75] Dayan S, Ozpazan NK, Özdemir N, et al. Synthesis of some ruthenium(II)-Schiff base complexes bearing sulfonamide fragment: New catalysts for transfer hydrogenation of ketones. *J Organomet Chem* 2014; 770: 21–28.
- [76] Ahn DU (Iowa SU. Chemical Properties of Amino Acids. *Org Chem Cl Notes* [http://www.public.iastate.edu/~duahn/teaching/Biomodulation and Protein/Amino Acids and peptide bond.pdf](http://www.public.iastate.edu/~duahn/teaching/Biomodulation%20and%20Protein/Amino%20Acids%20and%20peptide%20bond.pdf) (2016).

- [77] Technologies E. A COMPARITIVE VIEW OVER THE SYNTHESIS OF SCHIFF BASE LIGANDS AND METAL COMPLEXES BY CONVENTIONAL AND. 2017; 4: 107–117.
- [78] Liu J, Wu B, Zhang B, et al. Synthesis and characterization of heterocyclic Schiff base and its complexes with Cu (II), Ni (II), Co (II), Zn (II), and Cd (II). *Turkish J Chem* 2009; 62: 2728–2735.
- [79] Augustsson A. Accepted Manuscript. Epub ahead of print 2009. DOI: 10.1016/j.apgeochem.2009.04.028.
- [80] Rai BK, Kumari R. Synthesis , Structural , Spectroscopic and Antibacterial Studies of Schiff Base Ligands and their Metal Complexes.
- [81] Foster TJ. Staphylococcus aureus. *J Clin Invest* 2004; 114: 1693–96.
- [82] CDC. Antibiotic resistance threats in the United States, 2013. *Current* 2013; 114.
- [83] Das K, Tiwari RKS, Shrivastava DK. Techniques for evaluation of medicinal plant products as antimicrobial agents: current methods and future trends. *J Med Plants Res* 2010; 4: 104–111.
- [84] Baris Ö, Güllüce M, Şahın F, et al. Biological Activities of the Essential Oil and Methanol Extract of *Achillea biebersteinii* Afan.(Asteraceae). *Turkish J Biol* 2006; 30: 65–73.
- [85] Ncube NS, Afolayan AJ, Okoh AI, et al. Assessment techniques of antimicrobial properties of natural compounds of plant origin : current methods and future trends. *African J Biotechnol* 2008; 7: 1797–1806.
- [86] Rasmussen R V, Jr VGF, Skov R, et al. NIH Public Access. 2012; 6: 43–56.

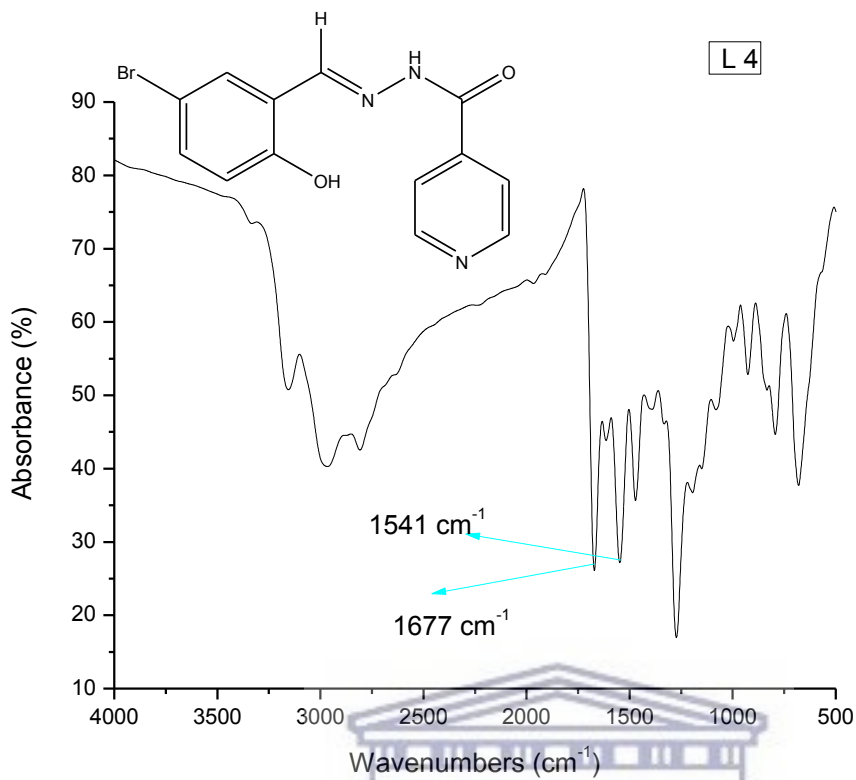
Appendix



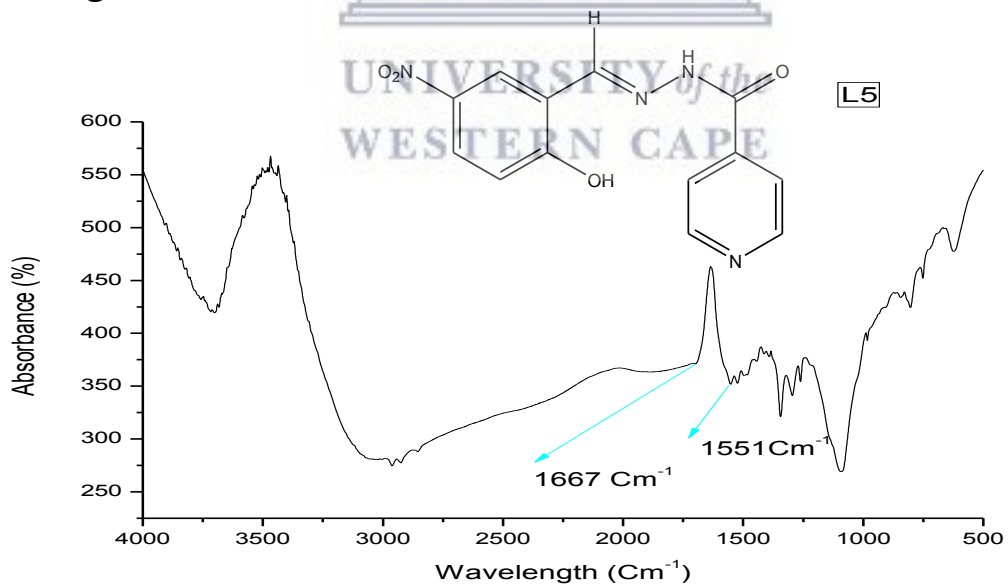
FTIR for ligand L2



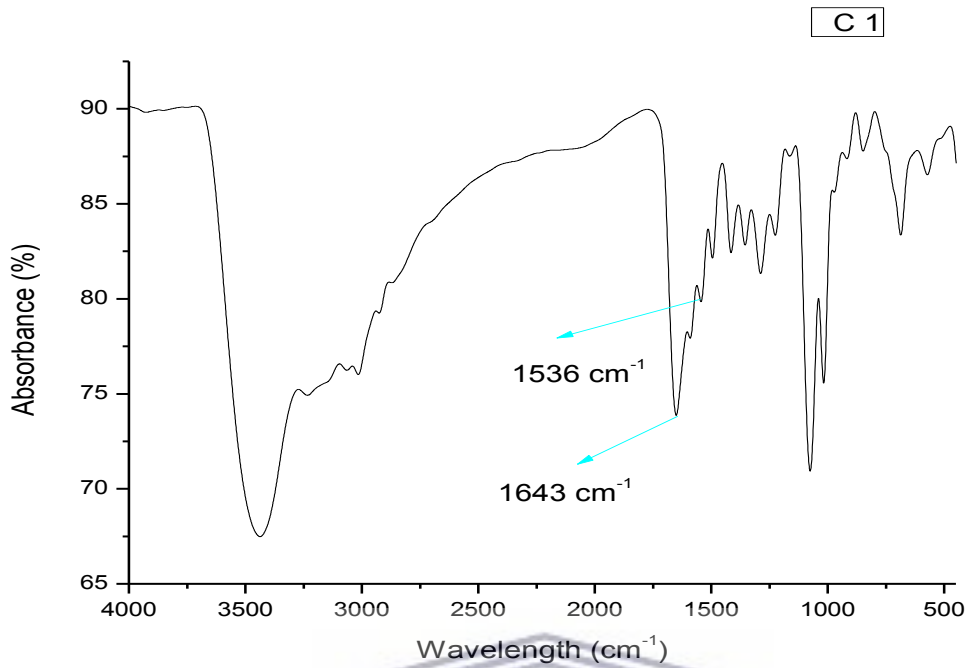
FTIR for ligand L3



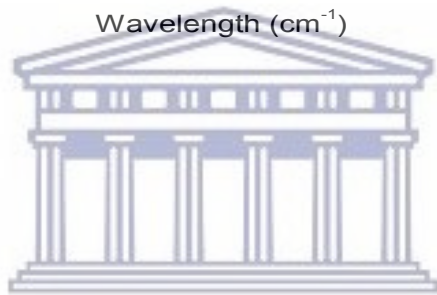
FTIR for ligand **L4**



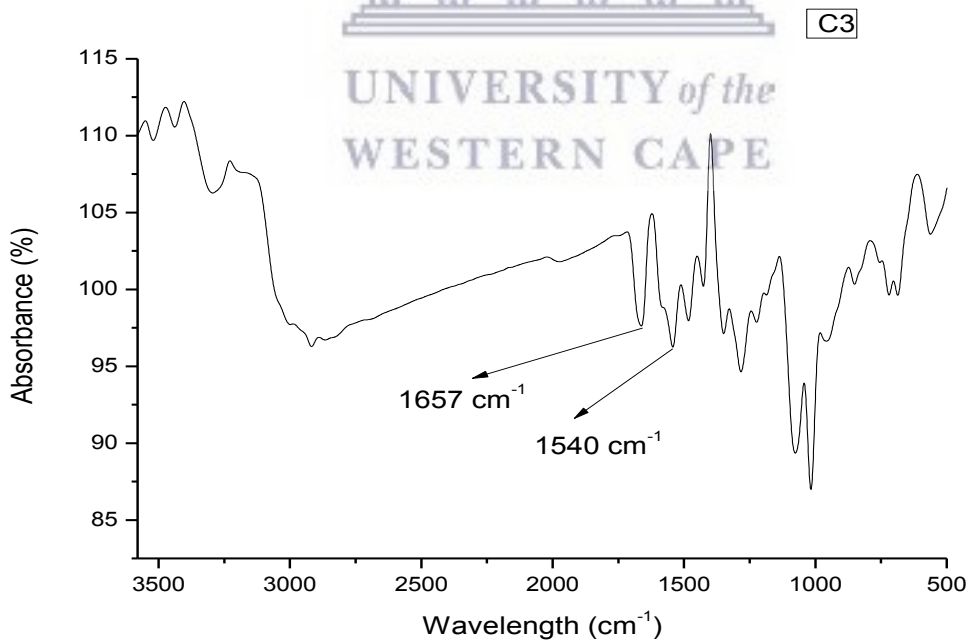
FTIR of ligand **L5**



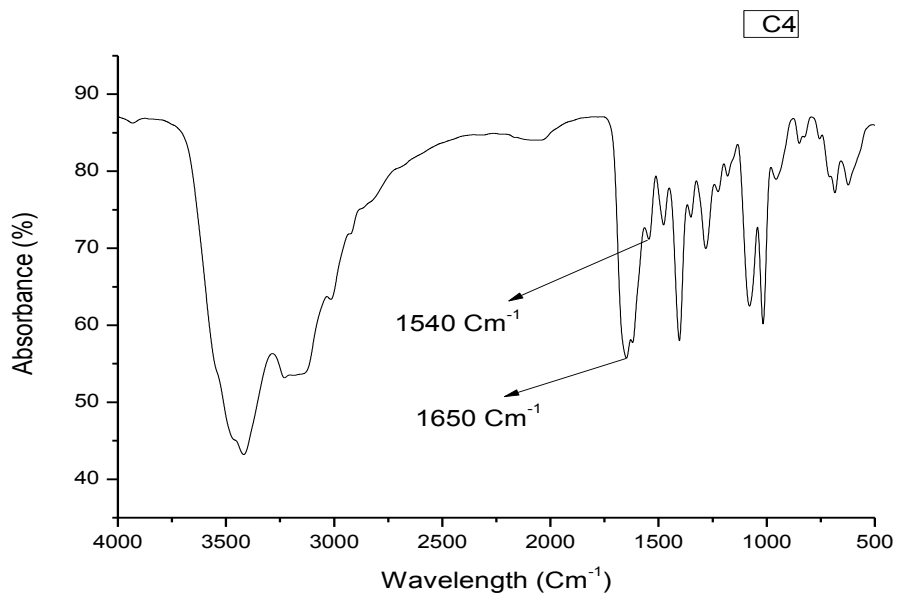
FTIR for complex **C1**



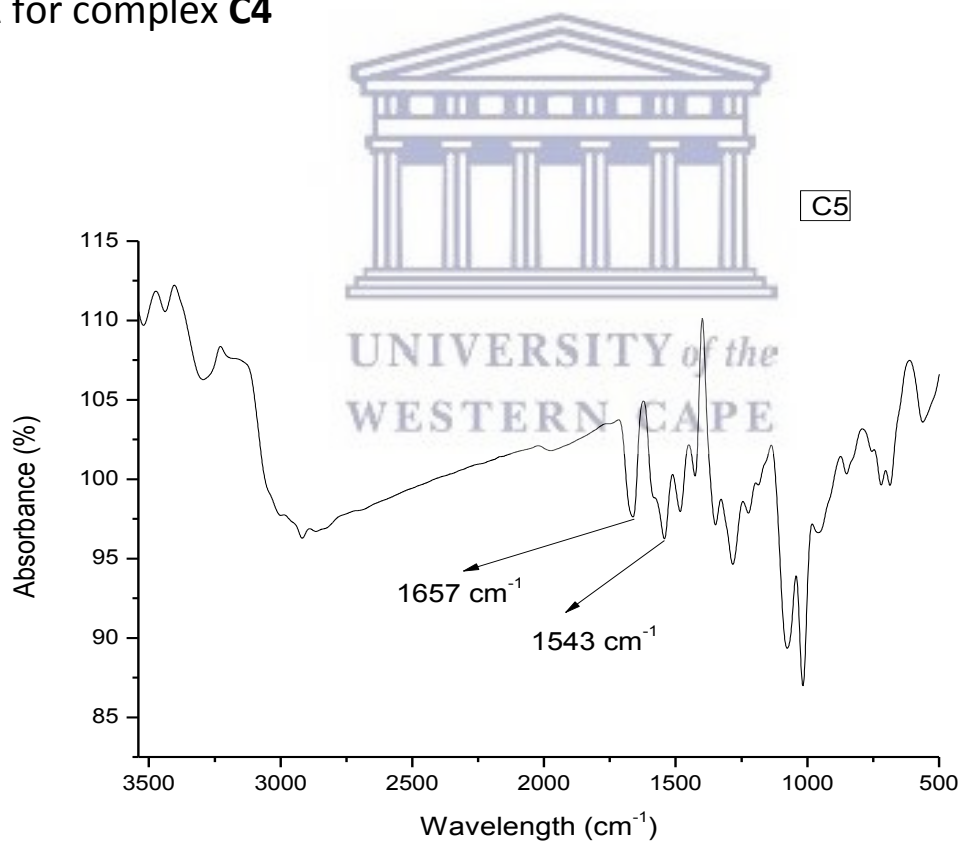
UNIVERSITY of the
WESTERN CAPE



FTIR for complex **C3**

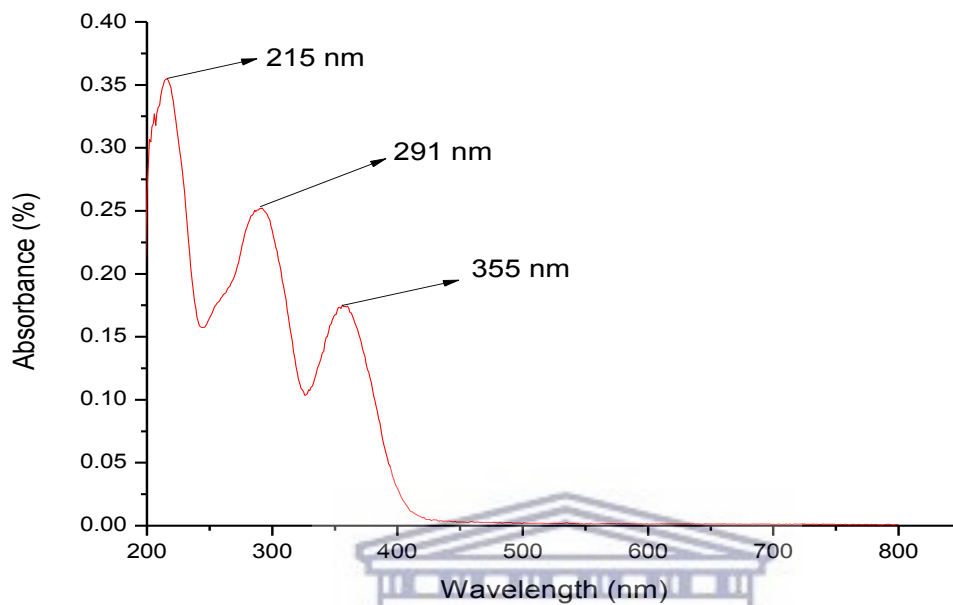


FTIR for complex **C4**

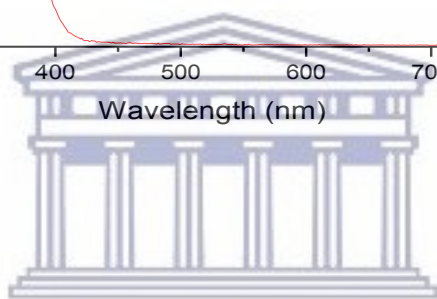


FTIR for complex **C5**

L 2

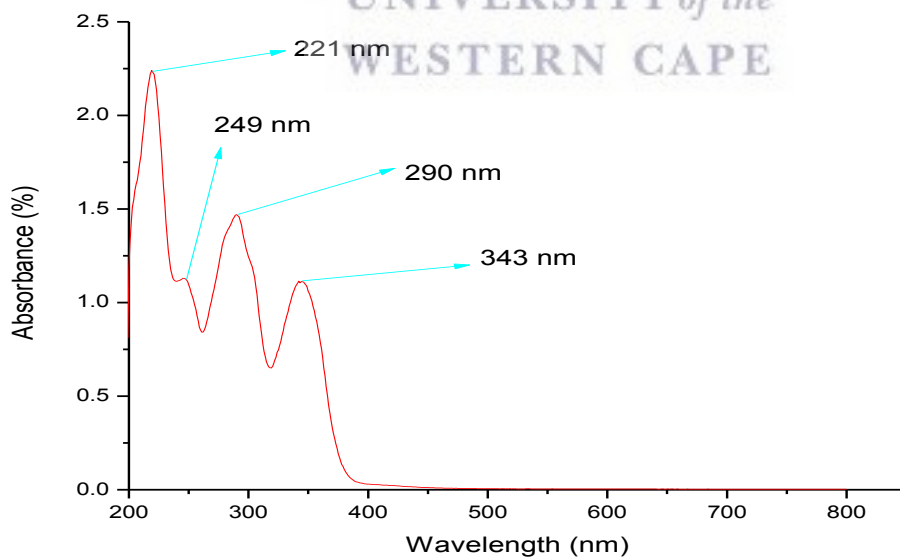


UV-VIS for ligand L2

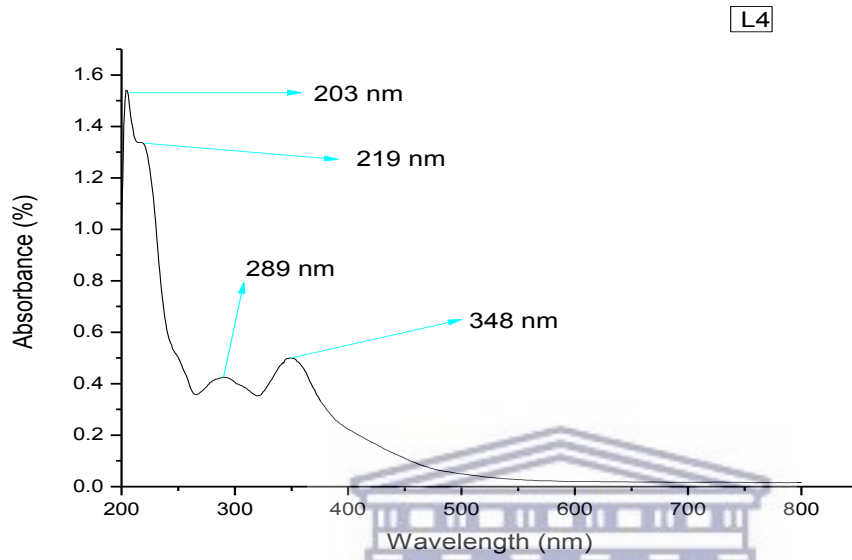


UNIVERSITY of the WESTERN CAPE

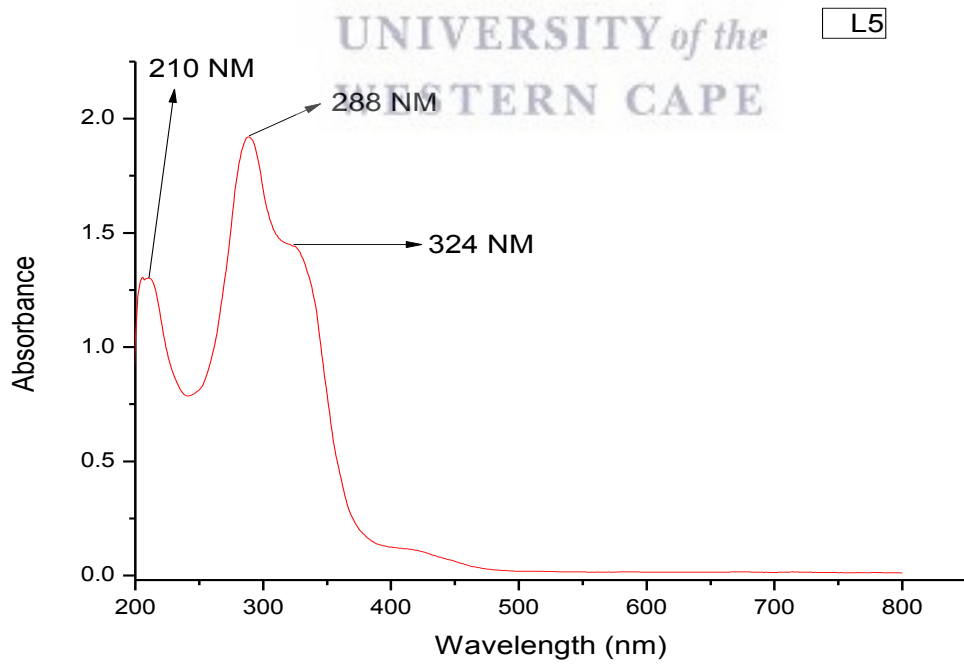
L 3



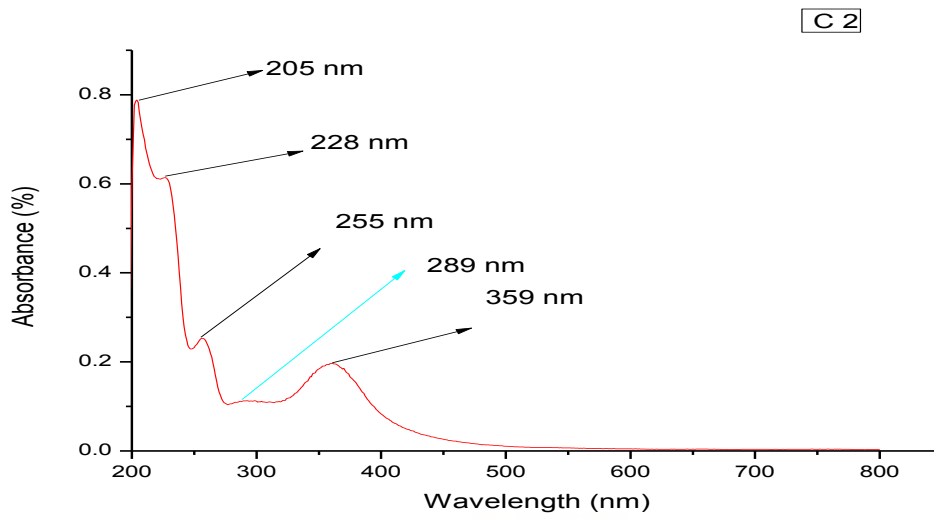
UV-VIS of ligand L3



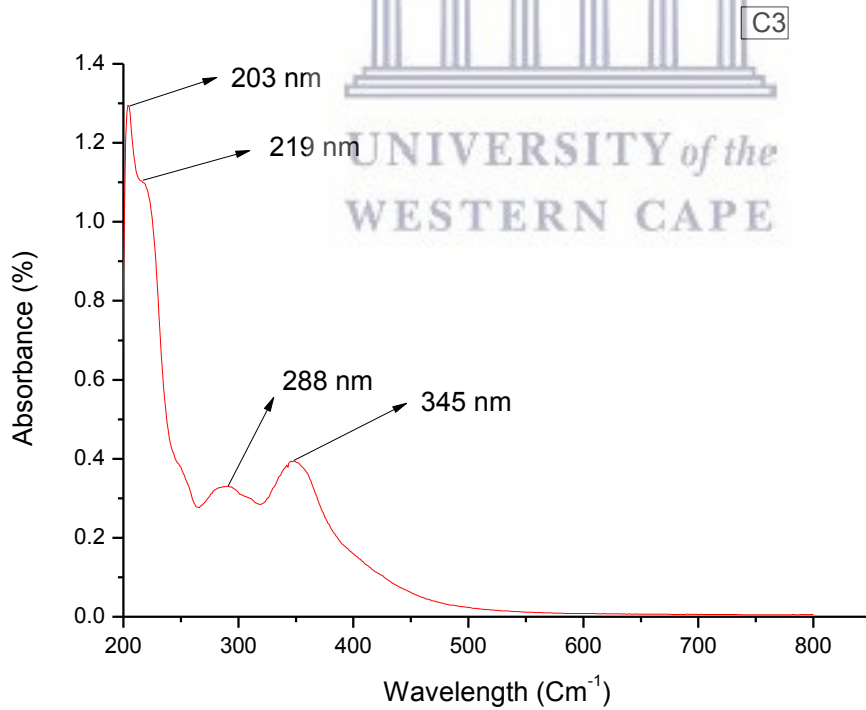
UV-VIS of ligand L4



UV-VIS of ligand L5

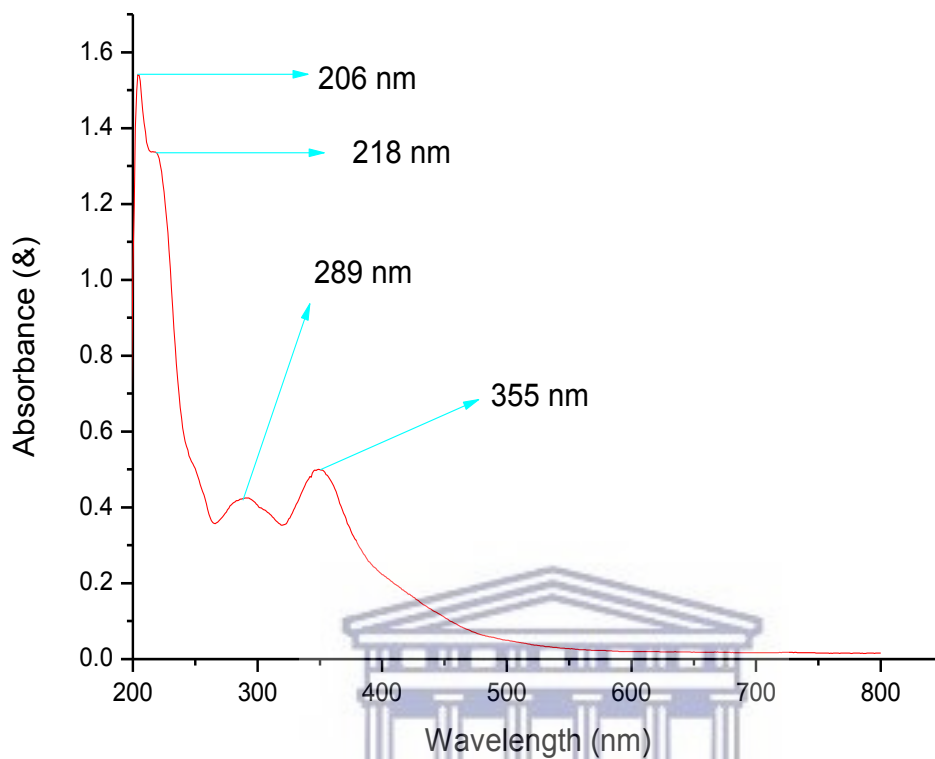


UV-VIS of complex C2

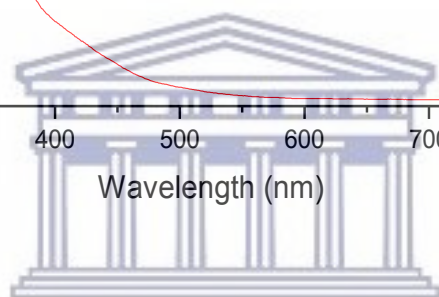


UV-VIS for complex C3

C 4

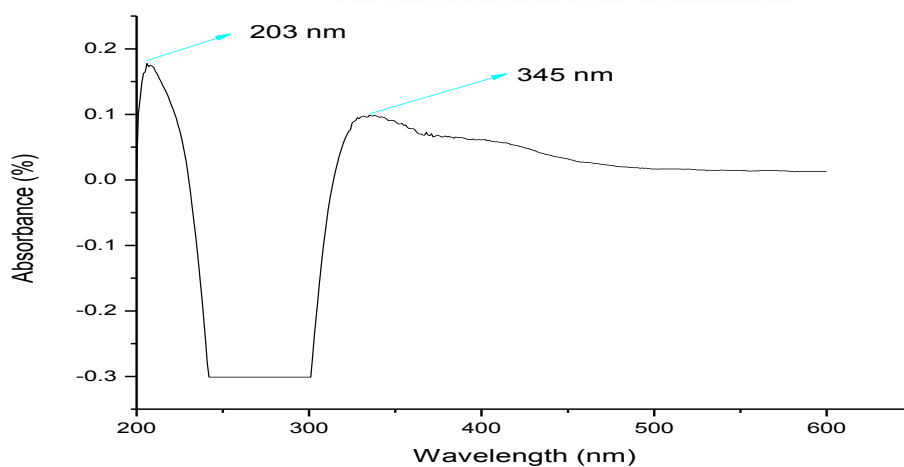


UV-VIS OF complex C4

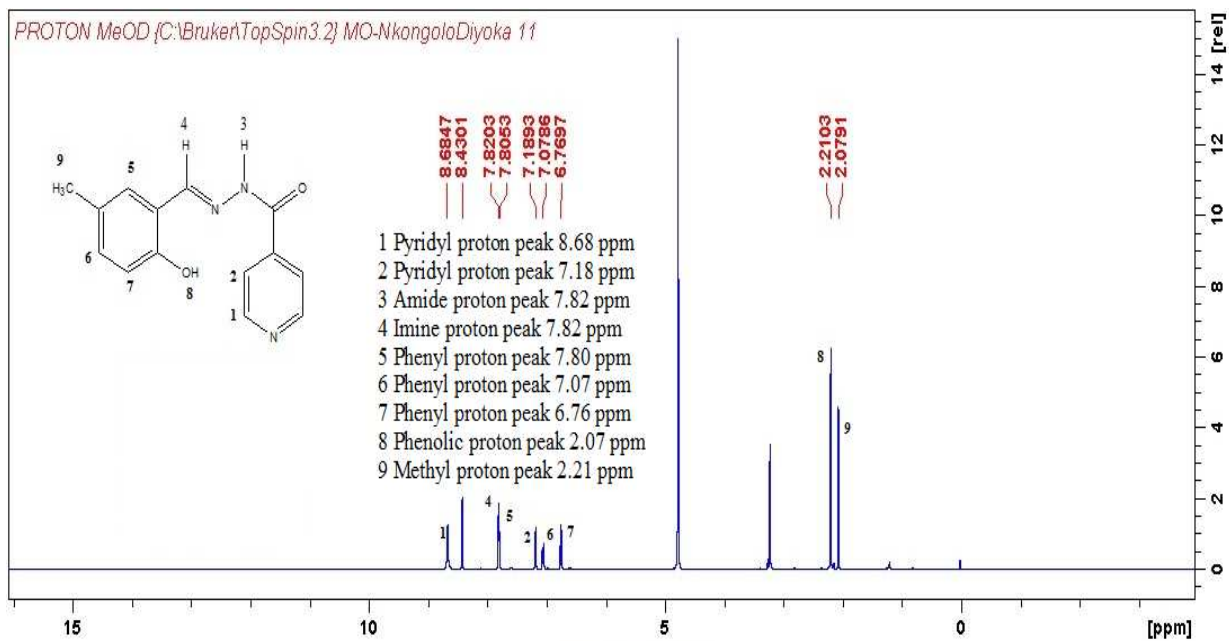


UNIVERSITY of the
WESTERN CAPE

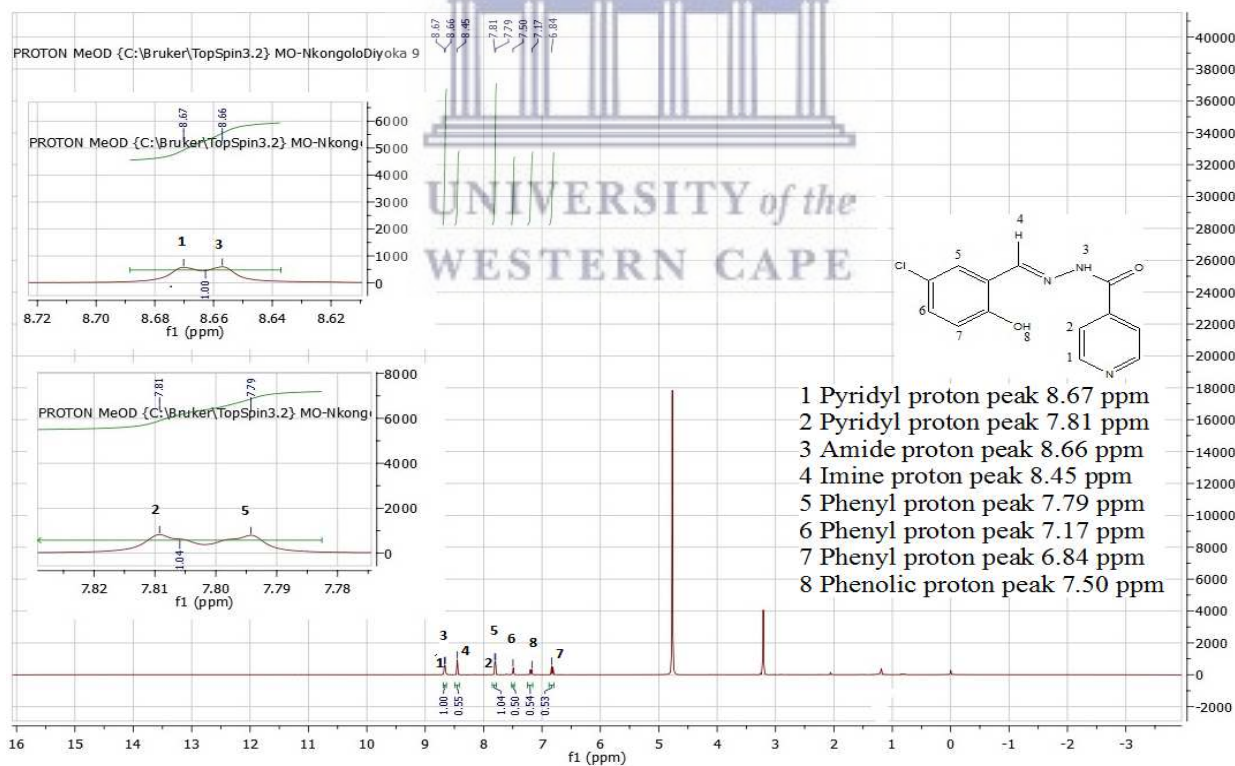
C5



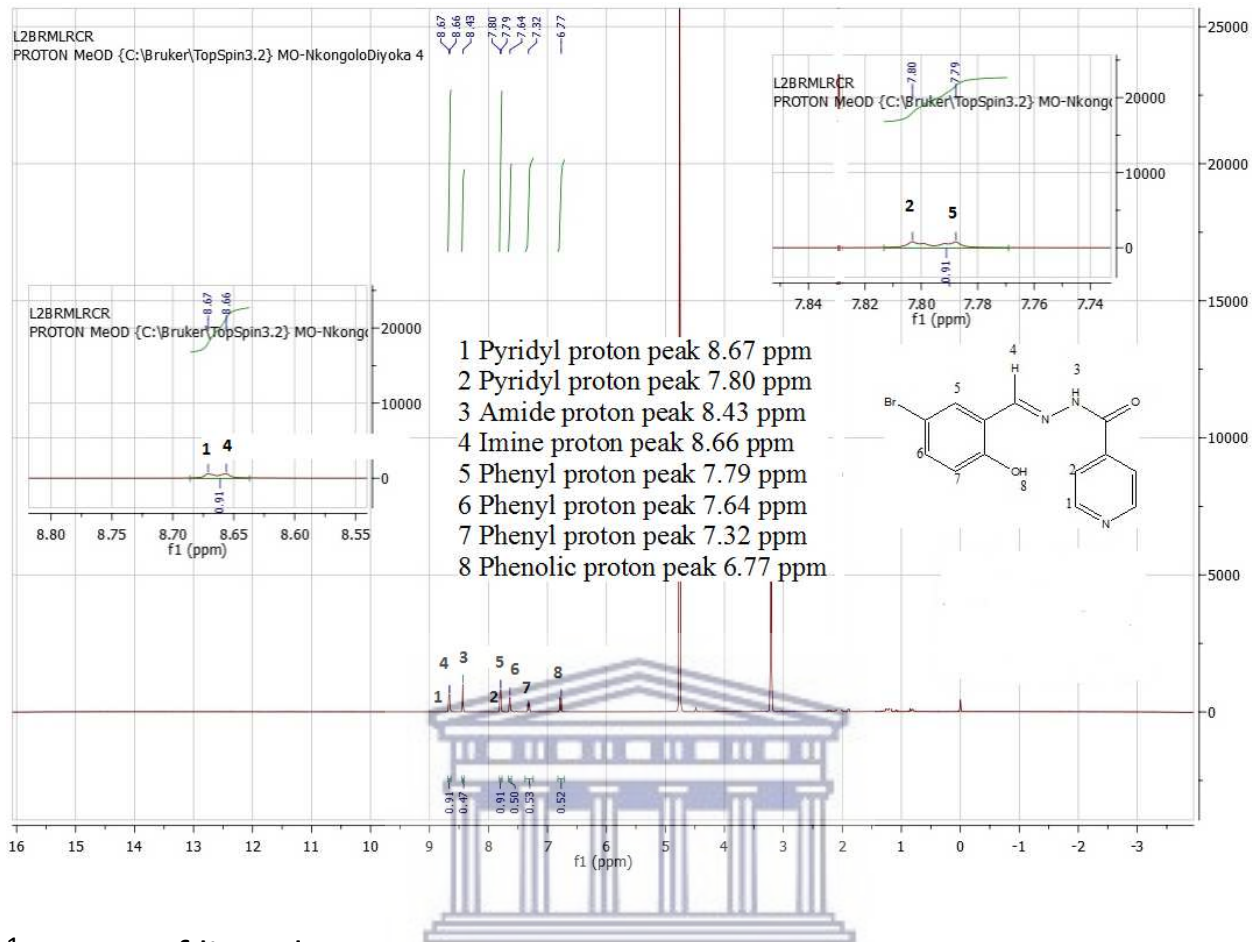
UV-VIS of complex C5



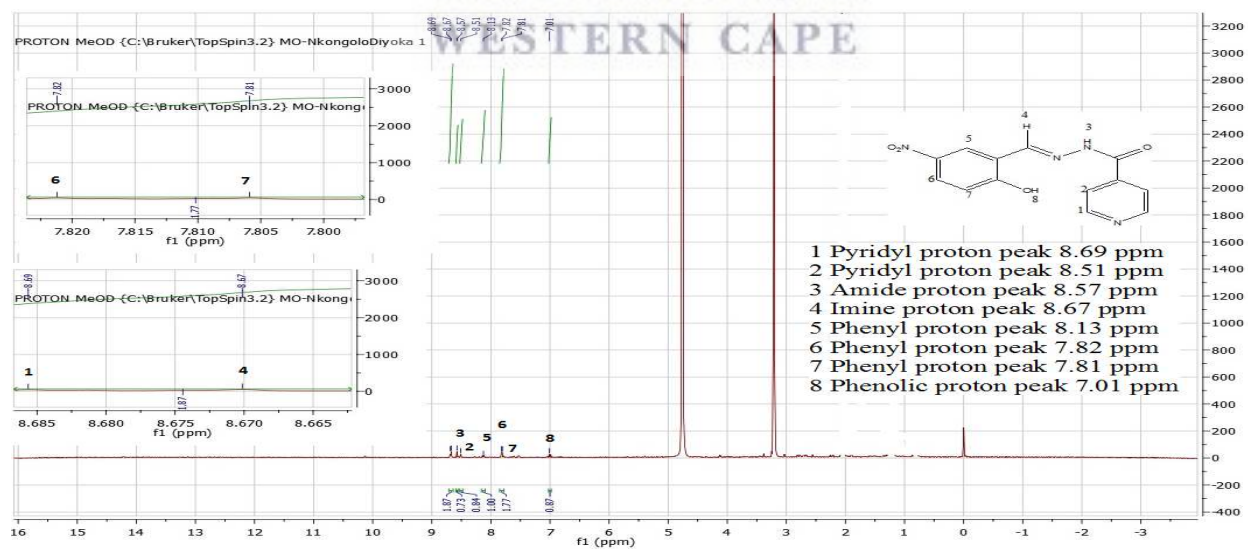
¹H NMR of ligand L1



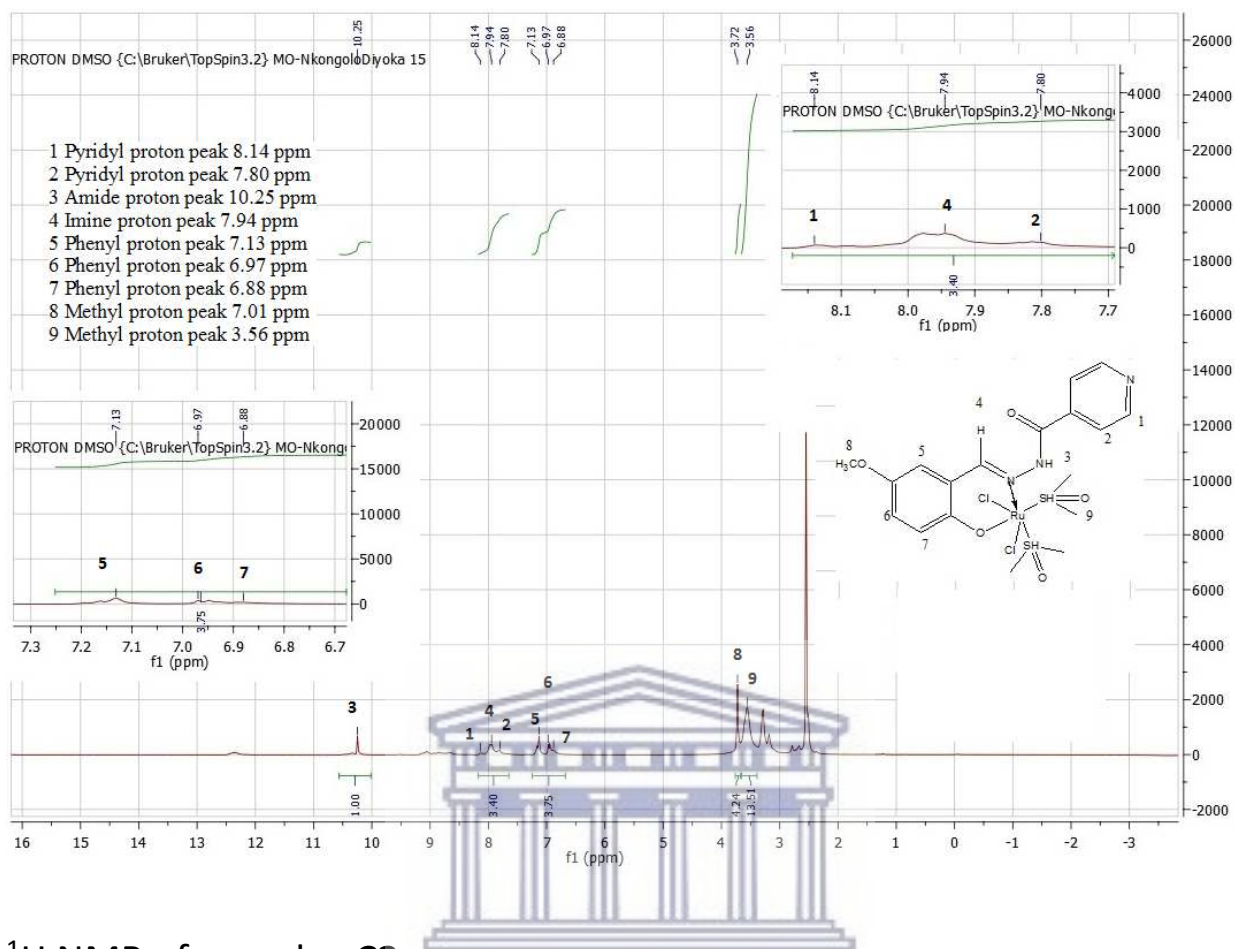
¹H NMR of ligand L3



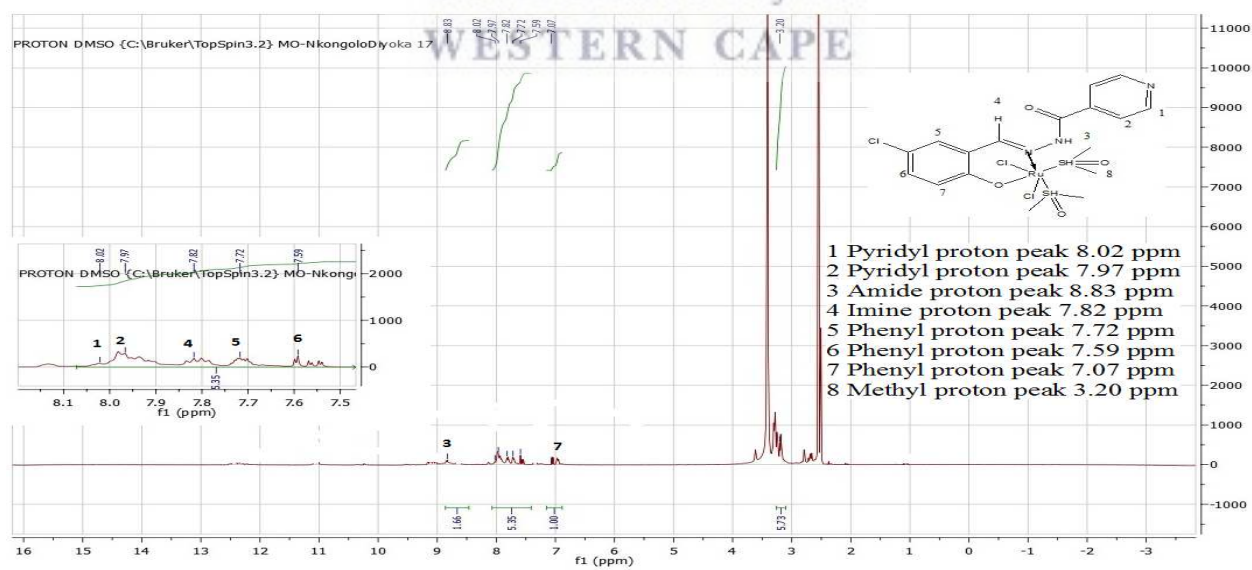
¹H NMR of ligand L4



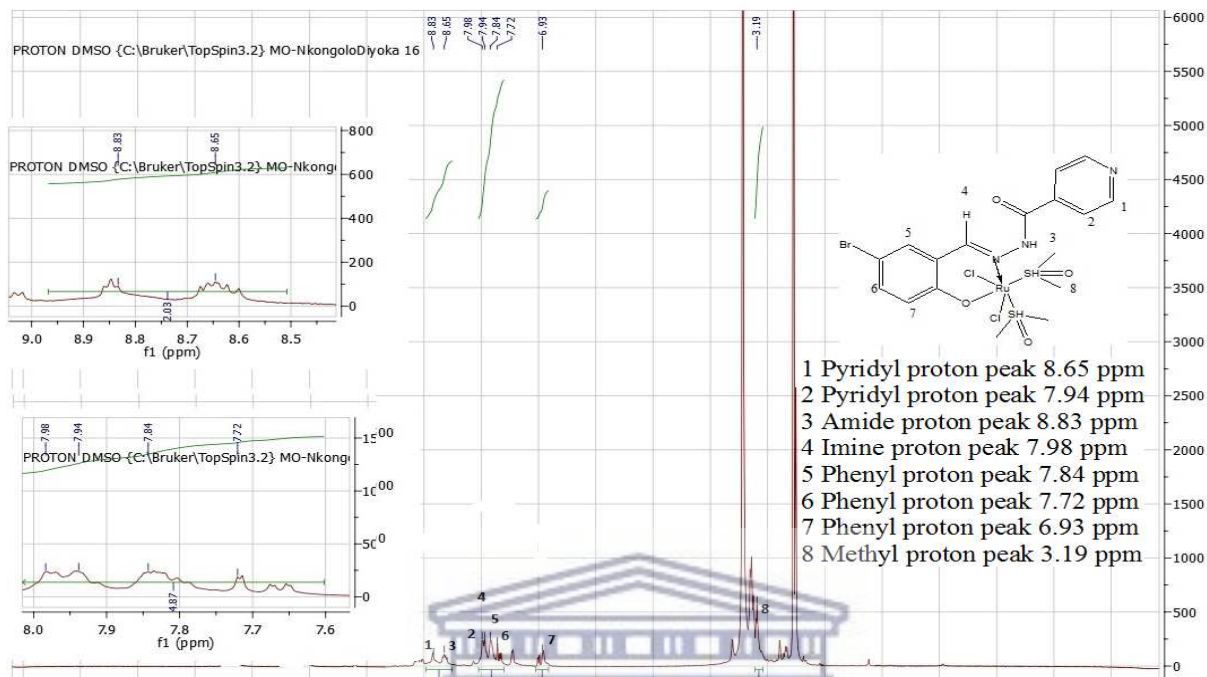
¹H NMR of ligand L5



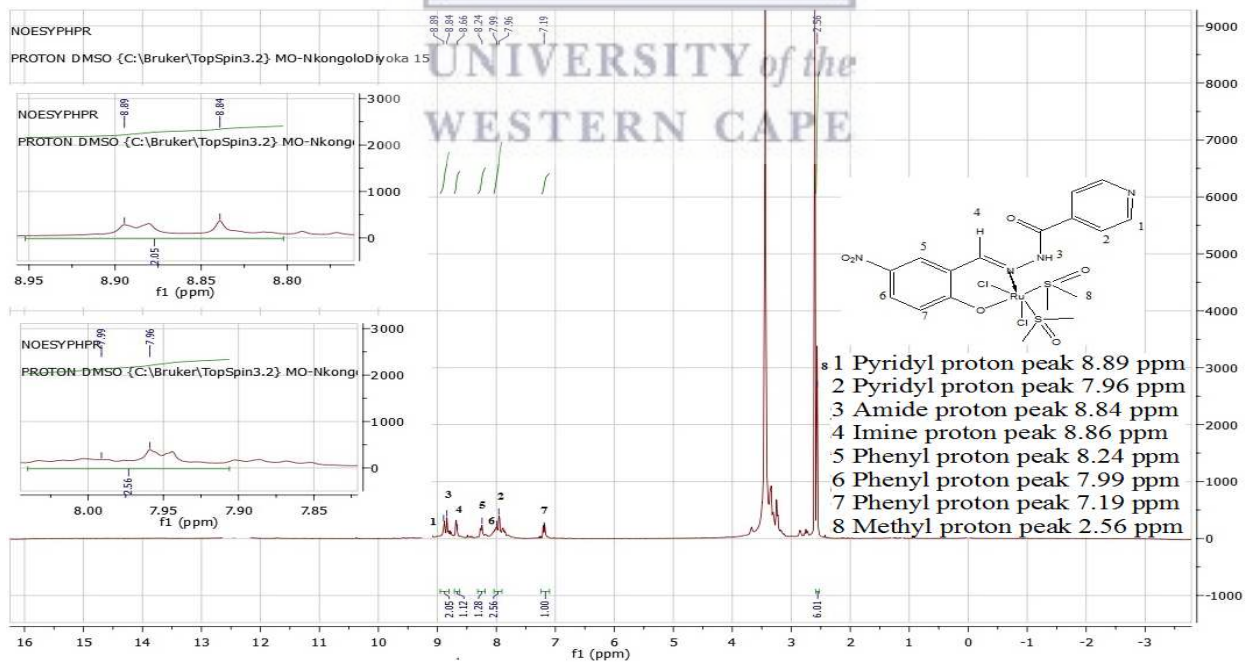
¹H NMR of complex C2



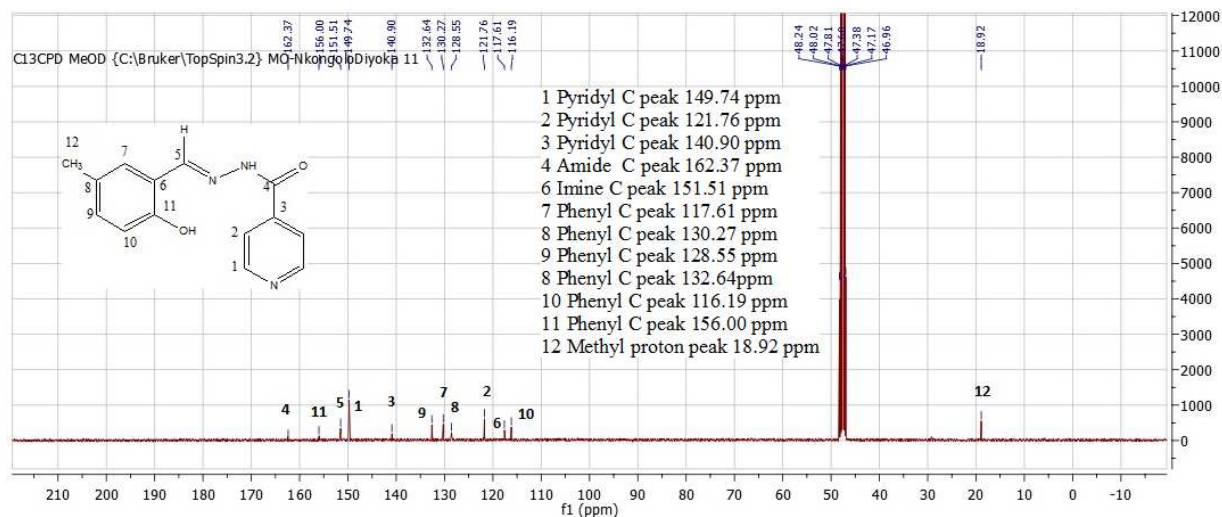
¹H NMR of complex C3



¹H NMR of complex C4

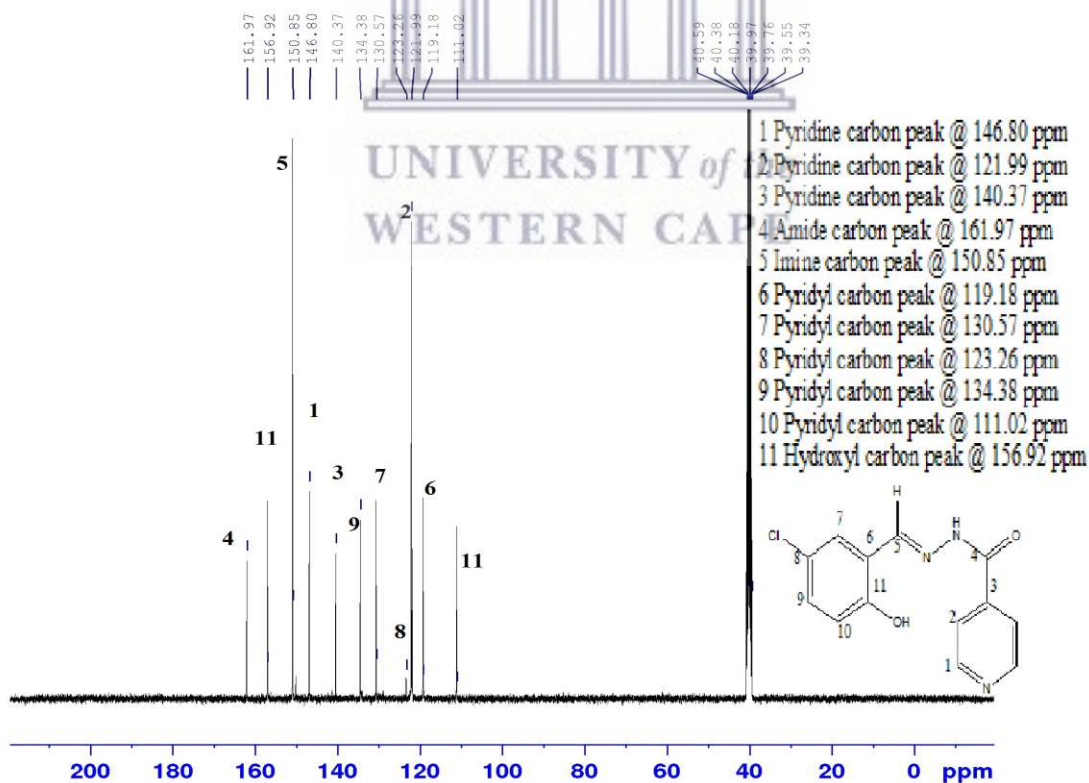


¹H NMR of complex C5

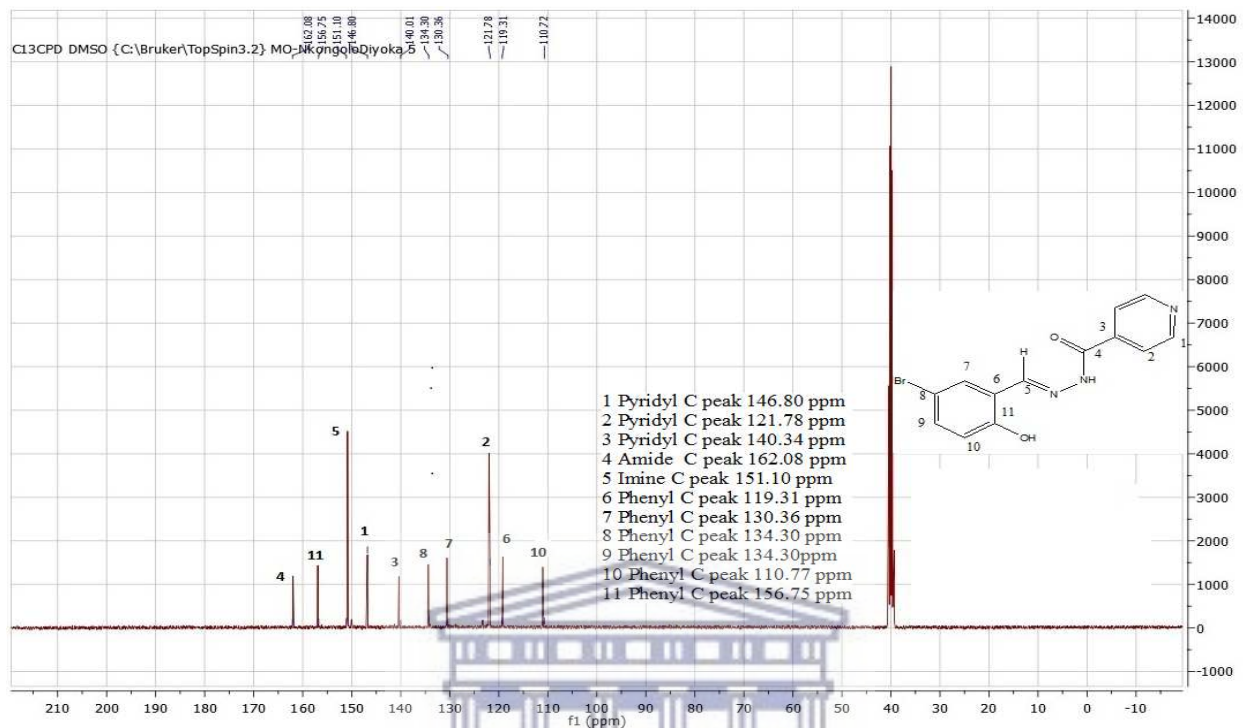


¹³C NMR peak of ligand L1

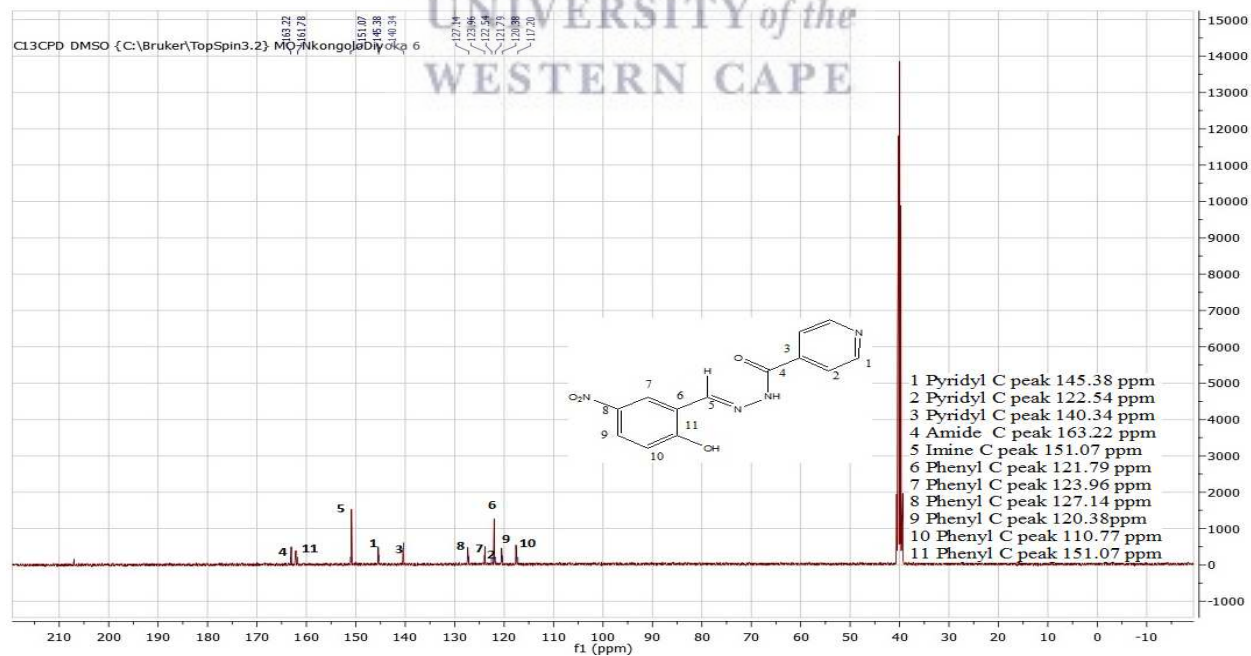
C13CPD DMSO {C:\Bruker\TopSpin3.2} MO-NkongoloDiyoka 5



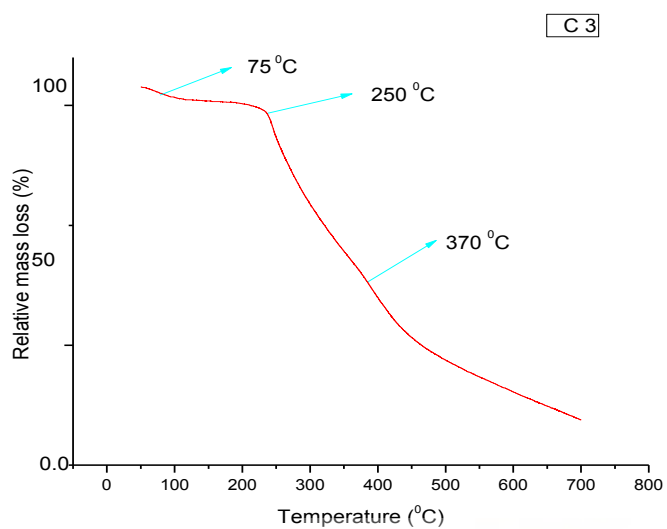
¹³C NMR of ligand L3



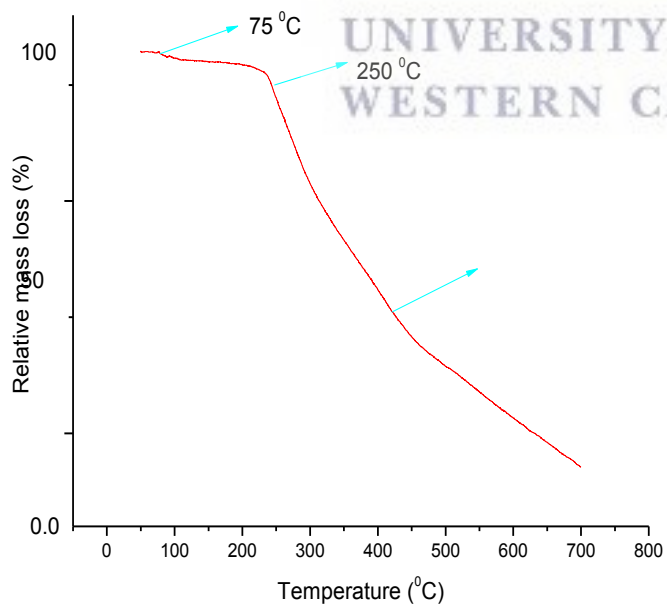
¹³C NMR of ligand C4



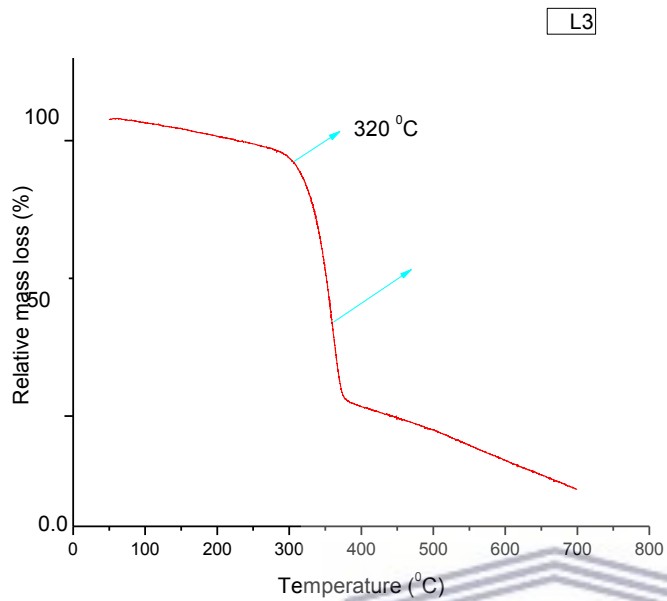
^{13}C NMR of ligand L5



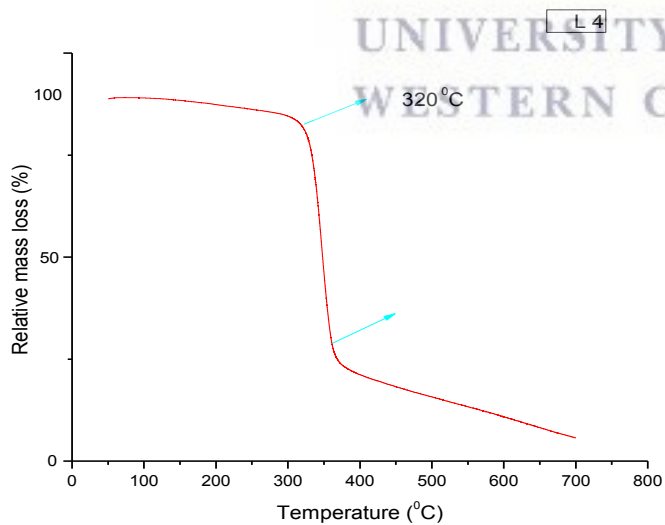
TGA graph of complex C3



TGA graph of complex C4



TGA graph of ligand L3



TGA graph of ligand L4